JCI The Journal of Clinical Investigation

Amendment history:
- Corrigendum (December 2021)

Constitutive activation of WASp in X-linked neutropenia renders neutrophils hyperactive

Marton Keszei, … , Scott B. Snapper, Lisa S. Westerberg

J Clin Invest. 2018;128(9):4115-4131. https://doi.org/10.1172/JCI64772.

Research Article **Immunology**

Graphical abstract

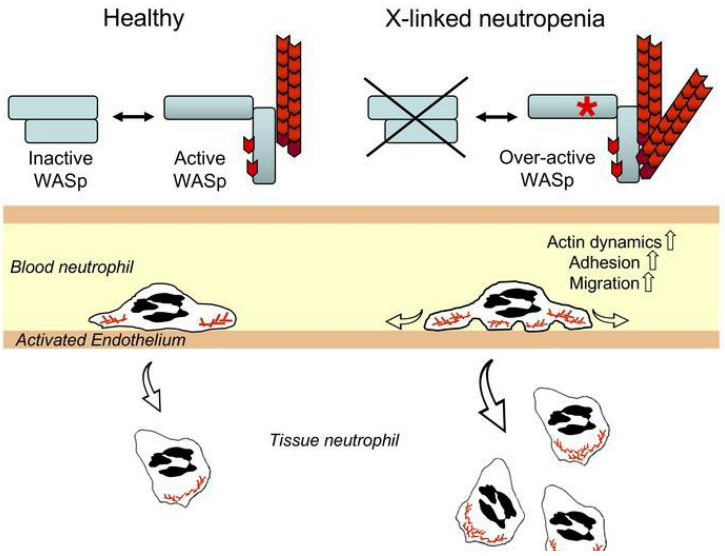

Constitutive activation of WASp in X-linked neutropenia renders neutrophils hyperactive

Marton Keszei,[1] Julien Record,[1] Joanna S. Kritikou,[1] Hannah Wurzer,[1] Chiara Geyer,[1] Meike Thiemann,[1] Paul Drescher,[1] Hanna Brauner,[1] Laura Köcher,[1] Jaime James,[1] Minghui He,[1] Marisa A.P. Baptista,[1] Carin I.M. Dahlberg,[1] Amlan Biswas,[2] Sonia Lain,[1] David P. Lane,[1] Wenxia Song,[3] Katrin Pütsep,[1] Peter Vandenberghe,[4] Scott B. Snapper,[2] and Lisa S. Westerberg[1]

[1]Department of Microbiology, Tumor and Cell Biology, Karolinska Institutet, Stockholm, Sweden. [2]Gastroenterology Division, Children's Hospital, Harvard Medical School, Boston, Massachusetts, USA. [3]Department of Cell Biology and Molecular Genetics, University of Maryland, College Park, Maryland, USA. [4]Center for Human Genetics, Katholieke Universiteit (KU) Leuven and Hematology/Internal Medicine, University Hospitals Leuven, Leuven, Belgium.

Congenital neutropenia is characterized by low absolute neutrophil numbers in blood, leading to recurrent bacterial infections, and patients often require life-long granulocyte CSF (G-CSF) support. X-linked neutropenia (XLN) is caused by gain-of-function mutations in the actin regulator Wiskott-Aldrich syndrome protein (WASp). To understand the pathophysiology in XLN and the role of WASp in neutrophils, we here examined XLN patients and 2 XLN mouse models. XLN patients had reduced myelopoiesis and extremely low blood neutrophil number. However, their neutrophils had a hyperactive phenotype and were present in normal numbers in XLN patient saliva. Murine XLN neutrophils were hyperactivated, with increased actin dynamics and migration into tissues. We provide molecular evidence that the hyperactivity of XLN neutrophils is caused by WASp in a constitutively open conformation due to contingent phosphorylation of the critical tyrosine-293 and plasma membrane localization. This renders WASp activity less dependent on regulation by PI3K. Our data show that the amplitude of WASp activity inside a cell could be enhanced by cell-surface receptor signaling even in the context in which WASp is already in an active conformation. Moreover, these data categorize XLN as an atypical congenital neutropenia in which constitutive activation of WASp in tissue neutrophils compensates for reduced myelopoiesis.

Introduction

Severe congenital neutropenia (SCN) is characterized by low absolute neutrophil count in blood that leads to life-threatening infections and requires administration of granulocyte CSF (G-CSF) to stimulate the number of circulating neutrophils (1–3). Mutations in ELA2/ELANE, HCLS1-associated protein X 1 (HAX1), adenylate kinase 2 (AK2), glucose-6-phosphate complex 3 (G6PC3), and Jagunal homolog 1 (JAGN1) cause SCN due to premature apoptosis of myeloid progenitor cells. Other genetic defects are associated with neutrophil dysfunction, such as mutations in the CYBB gene causing X-linked chronic granulomatous disease (CGD), in which NADPH oxidase fails to produce ROS and neutrophils are defective in killing bacteria (4), or mutations in the β_2 integrin family that cause leukocyte adhesion deficiency type I (LAD-I), characterized by lack of neutrophil transmigration through the activated endothelium (5).

The dynamics of the actin cytoskeleton are a critical feature of rapidly moving and acting cells, such as neutrophils. Local inflammation activates the endothelium, which upregulates P- and E-selectins that bind to glycosylated ligands on neutrophils, such as sialyl-Lewis^X and P-selectin glycoprotein ligand 1 (PSGL1) (6, 7). This allows fast-moving neutrophils in blood vessels to get tethered to the endothelial surface and start rolling along the vessel wall. Chemoattractants, such as formyl-peptides and CXCL1 (IL-8), activate β_2 integrin molecules on neutrophils that bind to ICAM-1 and -2 on the activated endothelium and mediate firm adhesion between neutrophils and the endothelium (6, 7). Neutrophil spreading is an essential step between crawling and arrest in the search for permissive sites to migrate through the endothelium into the tissue (8). In tissues, neutrophils use an amoeboid-type of migration characterized by intracellular polarization of the small Rho GTPases Rac2, Cdc42, and RhoA that gives rise to a leading edge lamellipodia in the front and a trailing uropod at the rear of the migrating cell. Failure to regulate the actin cytoskeleton impairs neutrophil number and function, as is demonstrated by mutations in the genes encoding for nonmuscular β-actin, the actin sensor megakaryoblastic leukemia 1 (MKL1), and the actin regulator Wiskott-Aldrich syndrome protein (WASp) (9–17).

The gene encoding WASp is uniquely expressed in hematopoietic cells and highly expressed during neutrophil maturation (Immgen.org). WASp is critically dependent on its structural conformation for activity and is predicted to reside in an inactive form in the cytoplasm caused by an intramolecular interaction between the GTPase-binding domain (GBD) and the C-terminal verprolin-cofilin-acidic (VCA) domain (18, 19). WASp binding to the small GTPase Cdc42 and phosphatidylinositol 4,5-bisphosphate (PIP2) releases autoinhibition and exposes the VCA domain to the Arp2/3 complex, which induces actin polymerization (18–20). The open conformation exposes the tyrosine Y291 (Y293 in mouse) in the GBD that, when phosphorylated, increases the basal activity of WASp toward the Arp2/3 complex,

Conflict of interest: The authors have declared that no conflict of interest exists.
Submitted: March 19, 2018; **Accepted:** July 3, 2018.
Reference information: *J Clin Invest*. 2018;128(9):4115–4131.
https://doi.org/10.1172/JCI64772.

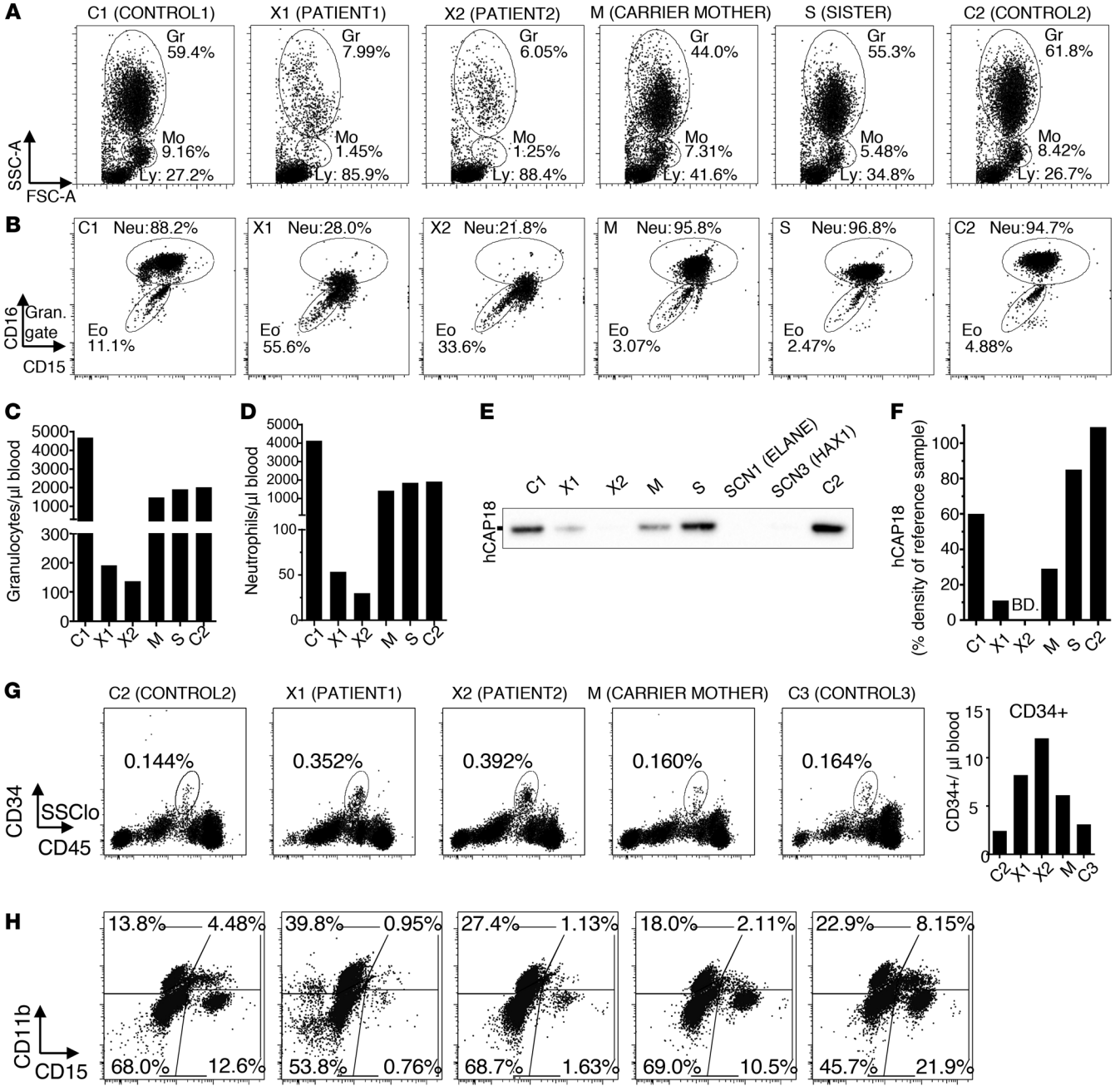

Figure 1. Severe neutropenia with hyperactivated neutrophils in the blood of XLN patients. (**A**) Forward and side scatter flow cytometry plots of RBC-lysed blood from WASp L270P XLN patients (X1 and X2), their mutation carrier mother (M), their sister with unknown carrier status (S), and 2 healthy male controls (C1 and C2). Granulocyte (Gr), monocyte (Mo), and lymphocyte (Ly) gates are marked with circles. (**B**) CD15 vs. CD16 staining of whole-blood granulocytes. Eo, eosinophils; Neu, neutrophils. (**C** and **D**) Granulocyte and neutrophil numbers in blood counted (from **A** and **B** populations) with flow cytometry using counting beads. (**E**) hCAP18 expression in serum as determined by Western blot. Serum from SCN1 (ELANE) and SCN3 (HAX1) patients served as references. (**F**) Densitometry of hCAP18 blots indicated as percentage density of 1 µg/ml hCAP18 reference sample. BD, below detection limit. (**G**) Percentage and number of CD34$^+$ hematopoietic progenitors in the blood of C2, X1, X2, M, and C3 (female control). (**H**) Composition of in vitro–differentiated myeloid liquid cultures from CD34$^+$ blood cells.

even upon dissociation from Cdc42 (21). In addition, phosphorylated WASp can be activated by Src family kinases and Tec family kinases, including Bruton's tyrosine kinase (Btk) (21–23).

The importance of WASp in hematopoietic cells is illustrated by 2 primary immunodeficiency syndromes, Wiskott-Aldrich syndrome (WAS) and X-linked neutropenia (XLN). WAS patients harbor loss-of-function mutations in WASp and suffer from eczema, microthrombocytopenia, and severe immunodeficiency, while XLN patients with gain-of-function mutations in the WASp GBD domain (L270P, S272P, or I294T) exhibit severe neutropenia and monocytopenia. XLN is considered an SCN; however, a puzzling clinical observation is that, despite an extremely low

number of circulating neutrophils (less than 0.3×10^9/l), XLN patients are generally not at high risk of infections and therefore do not require permanent G-CSF support (15). The lack of correlation between the circulating neutrophil number and rate of infections in XLN patients indicates that XLN should be distinguished from classical SCNs and requires more mechanistic understanding of the disease.

To understand how the activity of WASp needs to be regulated for normal neutrophil hematopoiesis, trafficking, and function, we here combined investigation of neutrophils from 2 XLN patients carrying the WASp L270P mutations with analysis of 2 mouse models harboring the corresponding human XLN mutations WASp L272P and WASp I296T. WASp L270P patients had defective myelopoiesis, which would predict a low peripheral neutrophil number; however, patients had normal neutrophil number in the saliva, suggesting a compensatory response for decreased bone marrow myeloid output. We found that neutrophils in WASp L272P and WASp I296T XLN mice were hyperactive in vitro and in vivo and showed that XLN is caused by hyperphosphorylated WASp that is constitutively recruited to the plasma membrane to induce actin dynamics. In this study, we provide mechanistic insight into clinical disease in XLN patients by showing that, despite decreased myelopoiesis, neutrophils are functional in tissues due to increased WASp activity, which is needed in all steps of neutrophil functionality.

Results

Low numbers of neutrophils in circulation and impaired hematopoiesis in XLN patients. To examine neutrophil granulocytes of WASp XLN patients, we collected blood from a previously described pedigree (16), including 2 brothers with the WASp L270P mutation (X1 and X2), their asymptomatic carrier mother (M), the sister with unknown carrier status (S), and from 2 healthy unrelated males serving as controls (C1 and C2). The numbers of granulocytes and monocytes and their ratios in the blood of X1 and X2 patients were dramatically decreased when compared with M, S, C1, and C2 (Figure 1, A–D, and Supplemental Figure 1, A and B; supplemental material available online with this article; https://doi.org/10.1172/JCI64772DS1). Consequently, the percentage of lymphocytes in the blood of XLN patients was high (Figure 1A), but the absolute lymphocyte number was normal (Supplemental Figure 1C). Granulocyte populations were divided into $CD15^{hi}$ $CD16^{hi}$ and $CD15^{lo}CD16^{lo}$ cells, corresponding to neutrophils and eosinophils in control samples, respectively (ref. 24 and Figure 1B). The numbers and ratios of neutrophils were severely reduced in X1 and X2 patients, and XLN neutrophils had low expression of CD16 (Figure 1B), indicating immaturity of granulocytes (24). Although the relative ratio of eosinophils to neutrophils was increased in XLN patients, the absolute eosinophil number was similar to that in controls (Supplemental Figure 1D). Gating on the neutrophil population, this population could be divided into $CD16^{hi}CD11b^{hi}$ and $CD16^{lo}CD11b^{hi}$ cells, corresponding to mature neutrophils/band cells and metamyelocytes, respectively (Supplemental Figure 1A). The control samples contained mostly mature neutrophils/band cells, while X1 and X2 samples contained a large proportion of metamyelocytes with reduced CD16 expression (Supplemental Figure 1A).

Human cathelicidin, hCAP18, is produced during myelopoiesis at the myelocyte stage of maturation. The disappearance of hCAP18 from serum is an indicator of myeloid maturation arrest in the bone marrow, as seen in SCN1, SCN3, and various bone marrow failure disorders (25, 26). We found that, compared with C1, C2, and S, X1 and M had reduced hCAP18 levels in serum samples and that levels were below detection limits in the X2 sample (Figure 1, E and F, and Supplemental Figure 1E). Healthy individuals have more than 40% hCAP18 in serum (25, 26), and M was just below the normal range (Figure 1E and Supplemental Figure 1E). This result indicates perturbed bone marrow myeloid maturation in the XLN patients.

We enriched $CD34^+$ stem cells and progenitor cells from the blood of XLN patients and healthy donors (Figure 1, G and H). Upon culturing $CD34^+$ cells in vitro with IL-3, SCF, and G-CSF, the proportion of $CD15^+CD11b^+$ neutrophils was lower in patients than in healthy controls (Figure 1H). M showed an intermediate phenotype (Figure 1H).

Since XLN patient neutrophils showed altered expression of surface molecules, we next examined granulocyte morphology by standard density gradient centrifugation and microscopy of blood cells (27). Corresponding to their reduced ratio by flow cytometry, XLN samples yielded 24-fold lower granulocytes/ml blood when compared with controls (C1, C2, M, and S). While the granulocyte-enriched preparation contained over 80% neutrophils in control samples, X1 and X2 preparations contained approximately equal proportions of nongranulocytes, eosinophils, and neutrophil-related cells (Supplemental Figure 1, F and G), indicating that, in the absence of neutrophils, nongranulocytes and eosinophils were enriched in the preparation. Manual counting of cell populations on cytospin images showed similar ratios (Supplemental Figure 1, H and I), as observed with flow cytometry.

Taking these data together, we observed that XLN patients have a reduced number of neutrophils in peripheral blood and defective myelopoiesis.

XLN neutrophils are hyperactivated in blood and are present in normal numbers in saliva. To examine the ultrastructural features of XLN neutrophils, we used transmission electron microscopy (TEM). When compared with C1 and C2 controls, X1 and X2 neutrophils showed an apparent reduction of electron-dense granules and had a more activated degranulated morphology (Figure 2A and Supplemental Figure 2A).

Further examination of neutrophils revealed 4- to 6-fold higher expression of Gp91phox, a marker of activation, on XLN neutrophils compared with controls before (Figure 2B) and after (Figure 2C) stimulation using PMA. This indicates that neutrophils were spontaneously activated in patients.

The reduced peripheral blood neutrophil number in SCN patients is often associated with severe periodontitis and gingivitis (1). However, no periodontal disease has been reported in XLN patients. We collected saliva samples from WASp L270P patients X1 and X2, the M, and C2 and C3 to examine neutrophils in saliva. Using imaging flow cytometry, we combined analysis of surface CD15 and CD45 staining and irregular nuclear morphology to identify neutrophils (Figure 2D). We found comparable numbers of neutrophils in control (C2, C3, M) and patient (X1, X2) samples (Figure 2D). When examined by toluidine blue staining and elec-

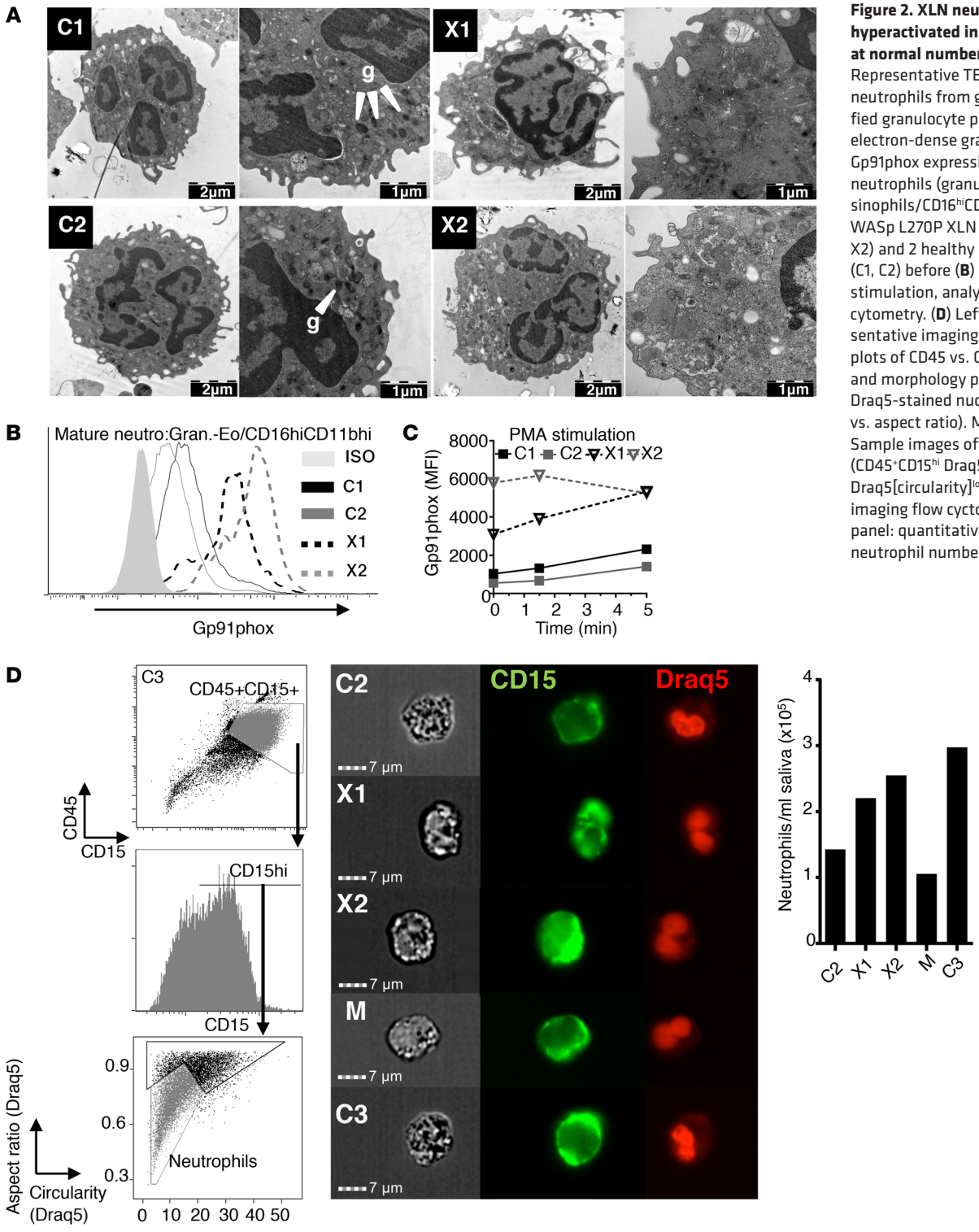

Figure 2. XLN neutrophils are hyperactivated in blood and are at normal numbers in saliva. (**A**) Representative TEM images of neutrophils from gradient-purified granulocyte preparation. g, electron-dense granules. (**B** and **C**) Gp91phox expression on mature neutrophils (granulocytes-eosinophils/CD16^{hi}CD11b^{hi}) from WASp L270P XLN patients (X1, X2) and 2 healthy male controls (C1, C2) before (**B**) or after (**C**) PMA stimulation, analyzed by flow cytometry. (**D**) Left panel: representative imaging flow cytometry plots of CD45 vs. CD15 staining and morphology parameters of Draq5-stained nuclei (circularity vs. aspect ratio). Middle panel: Sample images of neutrophils (CD45^{+}CD15^{hi} Draq5[aspect ratio]^{lo} Draq5[circularity]^{lo}) taken with imaging flow cyctometer. Right panel: quantitative analysis of neutrophil number/ml saliva.

tron microscopy, both control and XLN samples contained several cells with multilobular nucleus and granular (partially degranulated) cytoplasm. (Supplemental Figure 2, B and C). The presence of neutrophils in saliva suggests that XLN patient neutrophils have the capacity to migrate to the gingival tissues, thus protecting the oral site from periodontal diseases.

Murine WASp XLN is spontaneously phosphorylated and induces increased actin polymerization. To investigate how XLN mutations in WASp would affect neutrophil trafficking and function, we generated 2 new mouse models harboring the WASp L272P and the WASp I296T mutations (Figure 3A). The murine WASp L272P and I296T mutations correspond to human XLN mutations L270P and I294T and are part of the WASp GBD domain, with 100% amino acid identity in mice and humans. The WASp L272P and WASp I296T mice had normal neutrophil counts in bone marrow, blood, and spleen when compared with littermate WT controls (Supplemental Figure 3, A–C). Analysis of 1- to 2-year-old mice (Supplemental Figure 3, D and E) and of mice treated with G-CSF to stim-

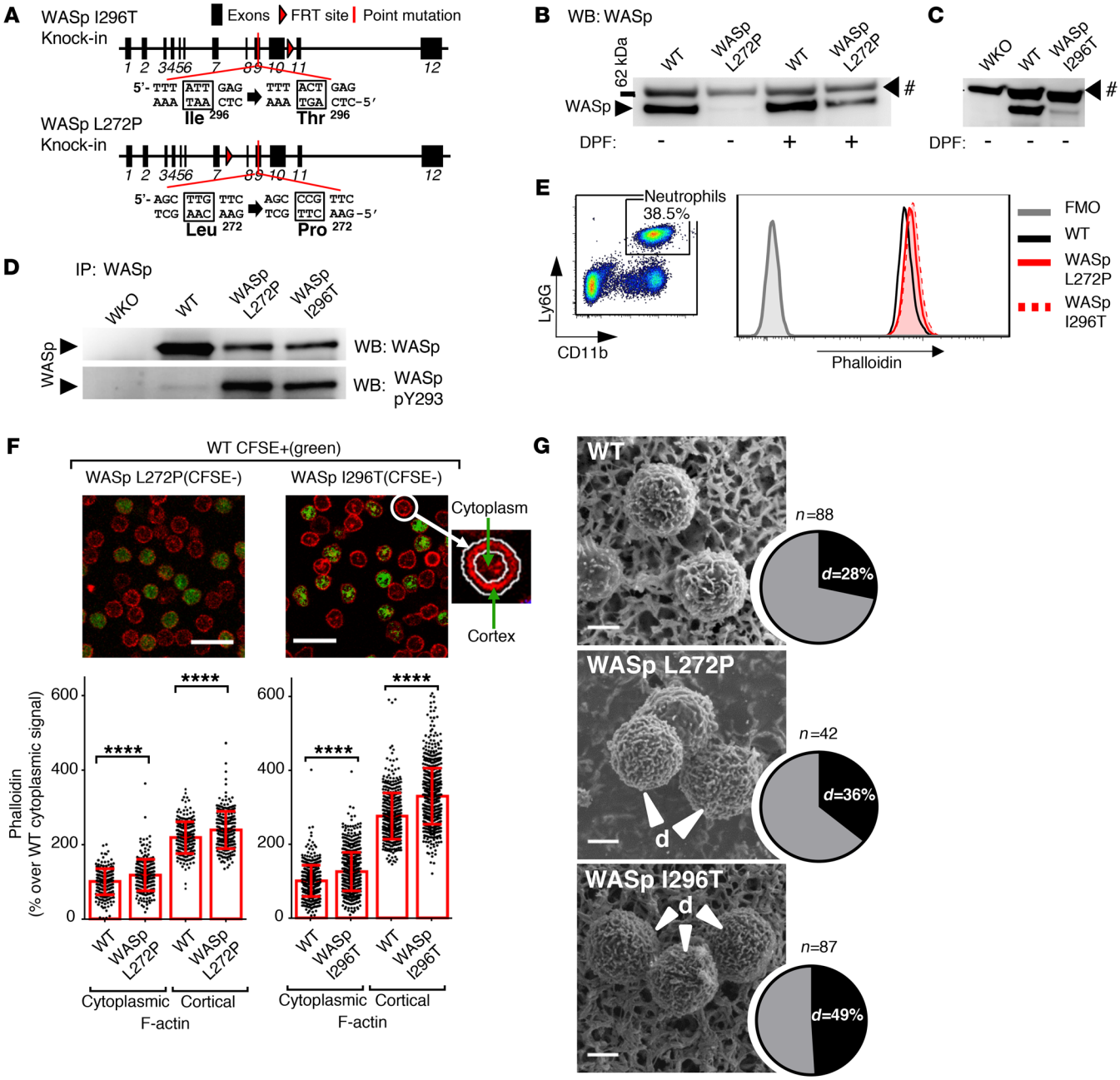

Figure 3. Increased polymerized actin, WASp Y293 phosphorylation, decreased WASp stability, and altered surface topography in mouse models of XLN. (**A**) Genomic organization, locations, and sequences of the introduced I296T and L272P mutations in the mouse *WASp* gene. (**B** and **C**) Protein expression of WASp in lysates of WT, WASp L272P, WASp I296T, and WASp-KO (WKO) peritoneal neutrophils with or without pretreatment of cells with DPF. WASp was detected by Western blotting (WB). #, unknown protein. n = 3 experiments. (**D**) Protein expression (upper panel) and Y293 phosphorylation (lower panel) of WASp in WKO, WT, WASp L272P, and WASp I296T in immunoprecipitated protein lysates of bone marrow neutrophils. n = 3 experiments. (**E**) FACS plot of $Ly6G^+CD11b^+$ neutrophils in mouse peripheral blood. F-actin content of neutrophils was measured with fluorescently labeled phalloidin and flow cytometry. A representative image of 3 individual blood samples per genotype is shown. (**F**) Quantitative analysis of cortical and cytoplasmic F-actin, labeled with phalloidin (red), in bone marrow neutrophils. Outlines of cells were recognized by Fiji software and the cortex defined by a ring encompassing the outline. Integrated fluorescent intensity in the ring area and within the ring were measured, and values from individual cells were plotted. CFSE labeling (for all genotypes both labeled and unlabeled samples) was used to differentiate between genotypes in each individual field. Data were normalized for the average of WT cytoplasmic signal (100%). Scale bars: 20 μM. WASp I296T (n = 752) vs. WT (n = 482); WASp L272P (n = 256) vs. WT (n = 231). Data are shown as mean ± SD. Unpaired, 2-tailed Student's t test. (**G**) Surface structure of WT, WASp L272P, and WASp I296T neutrophils. Cells were isolated from bone marrow, fixed in paraformaldehyde, and photographed with scanning electron microscopy. The percentages of cells with dense surface ruffles (d) were counted manually. Scale bars: 2 μM. $^{****}P < 0.0001$.

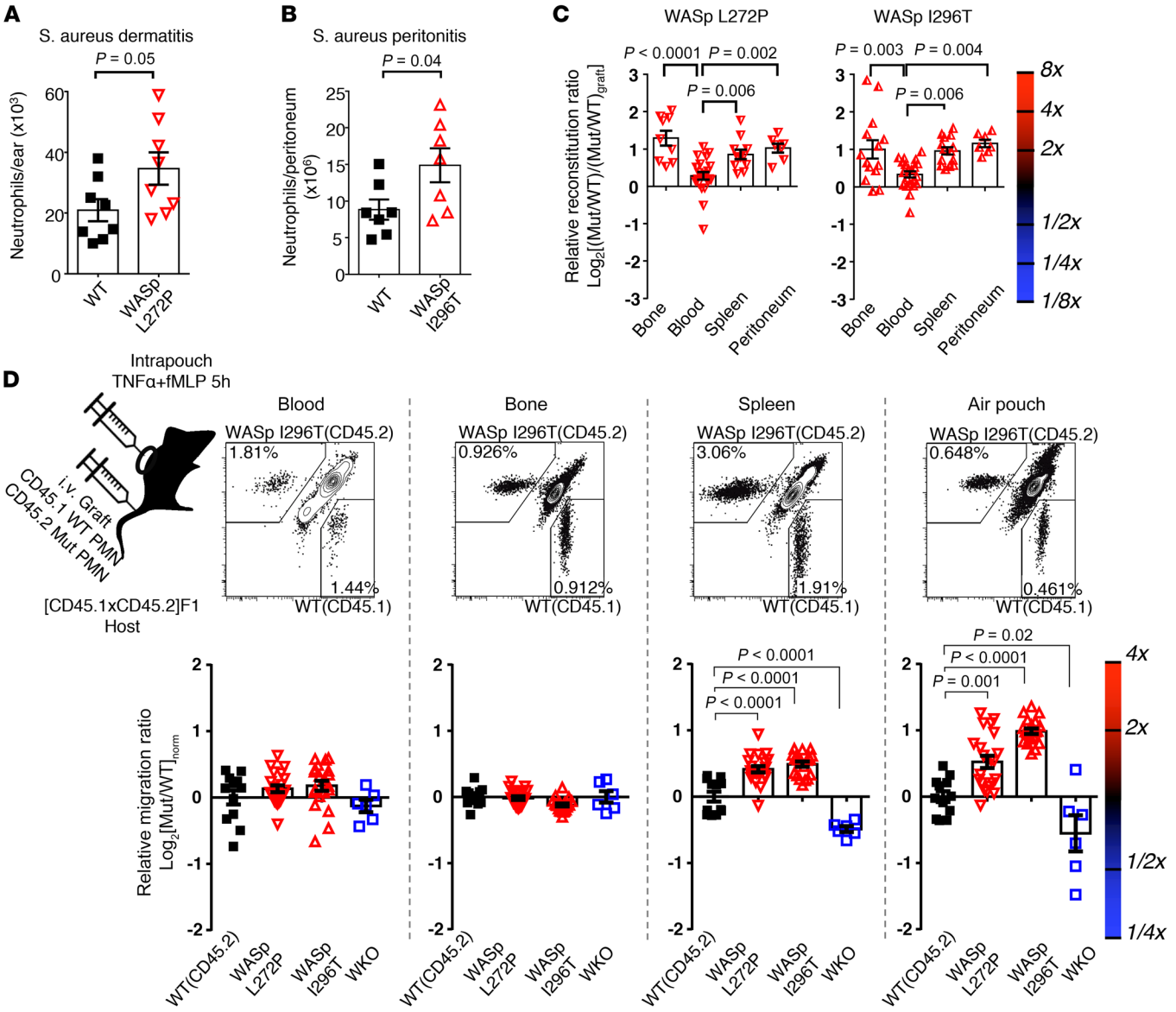

Figure 4. Increased rate of migration of WASp L272P and WASp I296T neutrophils to the spleen and to the inflammation site in vivo. (**A**) Neutrophil numbers in ears of WT and WASp L272P mice 6 hours after induction of dermatitis with *S. aureus* (10^6 CFU) injection. Data are shown as mean ± SEM. Unpaired, 2-tailed Student's *t* test. WT, *n* = 8; WASp L272P, *n* = 8/group. (**B**) WT and WASp I296T neutrophil numbers in peritoneum 24 hours after injection of *S. aureus* (20×10^6 CFU). Data are shown as mean ± SEM. Unpaired, 2-tailed Student's *t* test. WT, *n* = 7; WASp I296T, *n* = 7/group. (**C**) WASp L272P/CD45.1 WT (left panel) and WASp I296T/CD45.1 WT (right panel) neutrophil ratios in various organs in mixed bone marrow chimera mice were normalized with their original bone marrow reconstitution ratio (CD45.2/CD45.1) and plotted with logarithmic scale. Data are shown as mean ± SEM, 1-way ANOVA with Bonferroni's correction. WASp L272P/CD45.1: WT, *n* = 9 (bone); *n* = 22 (blood); *n* = 11 (spleen); *n* = 7 (peritoneum); WASp I296T/CD45.1: WT *n* = 14 (bone); *n* = 21 (blood); *n* = 14 (spleen); *n* = 7/group (peritoneum). (**D**) In vivo homing of WASp L272P (CD45.2), WASp I296T (CD45.2), and CD45.1 WT cells into various tissues was measured 5 hours after i.v. injection of bone marrow neutrophil grafts. Graft neutrophils ($CD45.1^+$ or $CD45.2^+$ single positive) were counted in blood, bone marrow, spleen, and air pouch lavage. The normalization formula is explained in Methods. Pool of at least 2 experiments per genotype. Data are shown as mean ± SEM, 1-way ANOVA with Bonferroni's correction. WT, *n* = 12; WASp I296T, *n* = 20; WASp L272P, *n* = 21; WKO, *n* = 6/group.

ulate myelopoiesis (Supplemental Figure 3, F–H) showed similar neutrophil counts in WASp L272P, WASp I296T, and WT mice. As predicted by the autoinhibited regulation of WASp (16, 18), neutrophil WASp L272P and WASp I296T were prone to degradation by neutrophil serine proteases in vitro when compared with WT WASp (Figure 3, B and C, and Supplemental Figure 3, I and J). WASp L272P and WASp I296T were spontaneously phosphorylated at Y293, while WT WASp showed only a weak phosphorylation signal (Figure 3D and Supplemental Figure 3, K and L). Despite protease inhibitor treatment, Y293-phosphorylated proteolytic fragments were detected in the XLN samples (Supplemental Figure 3, K and L). WASp L272P and WASp I296T neutrophils had increased F-actin content compared with WT neutrophils, as assessed by flow cytometry (Figure 3E). To analyze the distribu-

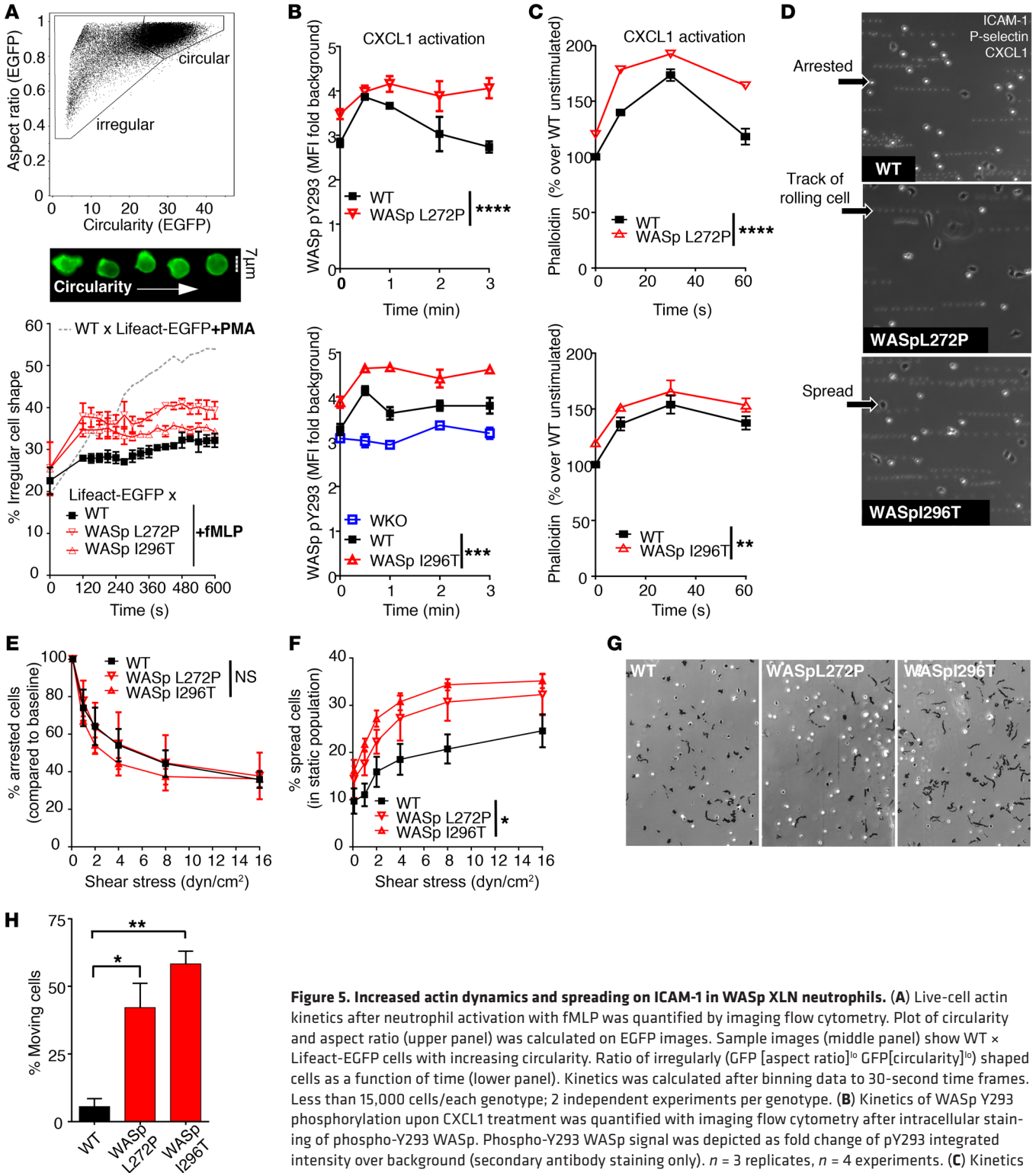

Figure 5. Increased actin dynamics and spreading on ICAM-1 in WASp XLN neutrophils. (**A**) Live-cell actin kinetics after neutrophil activation with fMLP was quantified by imaging flow cytometry. Plot of circularity and aspect ratio (upper panel) was calculated on EGFP images. Sample images (middle panel) show WT × Lifeact-EGFP cells with increasing circularity. Ratio of irregularly (GFP [aspect ratio]^{lo} GFP[circularity]^{lo}) shaped cells as a function of time (lower panel). Kinetics was calculated after binning data to 30-second time frames. Less than 15,000 cells/each genotype; 2 independent experiments per genotype. (**B**) Kinetics of WASp Y293 phosphorylation upon CXCL1 treatment was quantified with imaging flow cytometry after intracellular staining of phospho-Y293 WASp. Phospho-Y293 WASp signal was depicted as fold change of pY293 integrated intensity over background (secondary antibody staining only). n = 3 replicates, n = 4 experiments. (**C**) Kinetics of F-actin polymerization upon CXCL1 treatment was quantified with phalloidin staining and flow cytometry. n = 3 replicates, n = 3 experiments. (**D**) rmP-selectin–, rmICAM-1–, and rmCXCL-1–coated plastic flow chambers were perfused with bone marrow neutrophils at 0.1 dyn/cm^2. Representative images were taken after increasing flow rate to 2 dyn/cm^2. Motility was assessed by overlaying 10 consecutive frames. (**E**) Number of arrested cells were counted and depicted as percentage of arrested cells at 0.1 dyn/cm^2 after increasing flow rate stepwise with 30 seconds of run at each indicated sheer stress. n = 3 replicates, n = 3 experiments. (**F**) Ratio of spread cells at increasing flow rate. (**G**) Neutrophils in rmP-selectin–, rmICAM-1–, and rmCXCL-1–coated plastic flow chambers at 2 dyn/cm^2 shear stress. Black tracks indicate the motility of adherent cells within a 20-minute time period. n = 3 images/genotype. Data are represented as mean ± SEM. One-way (**H**) or 2-way ANOVA (**B**, **C**, **E**, **F**) and Bonferroni's multiple comparison test were used statistical significance. *P < 0.05; **P < 0.01; ***P < 0.001; ****P < 0.0001. Original magnification: ×100 (**D** and **G**).

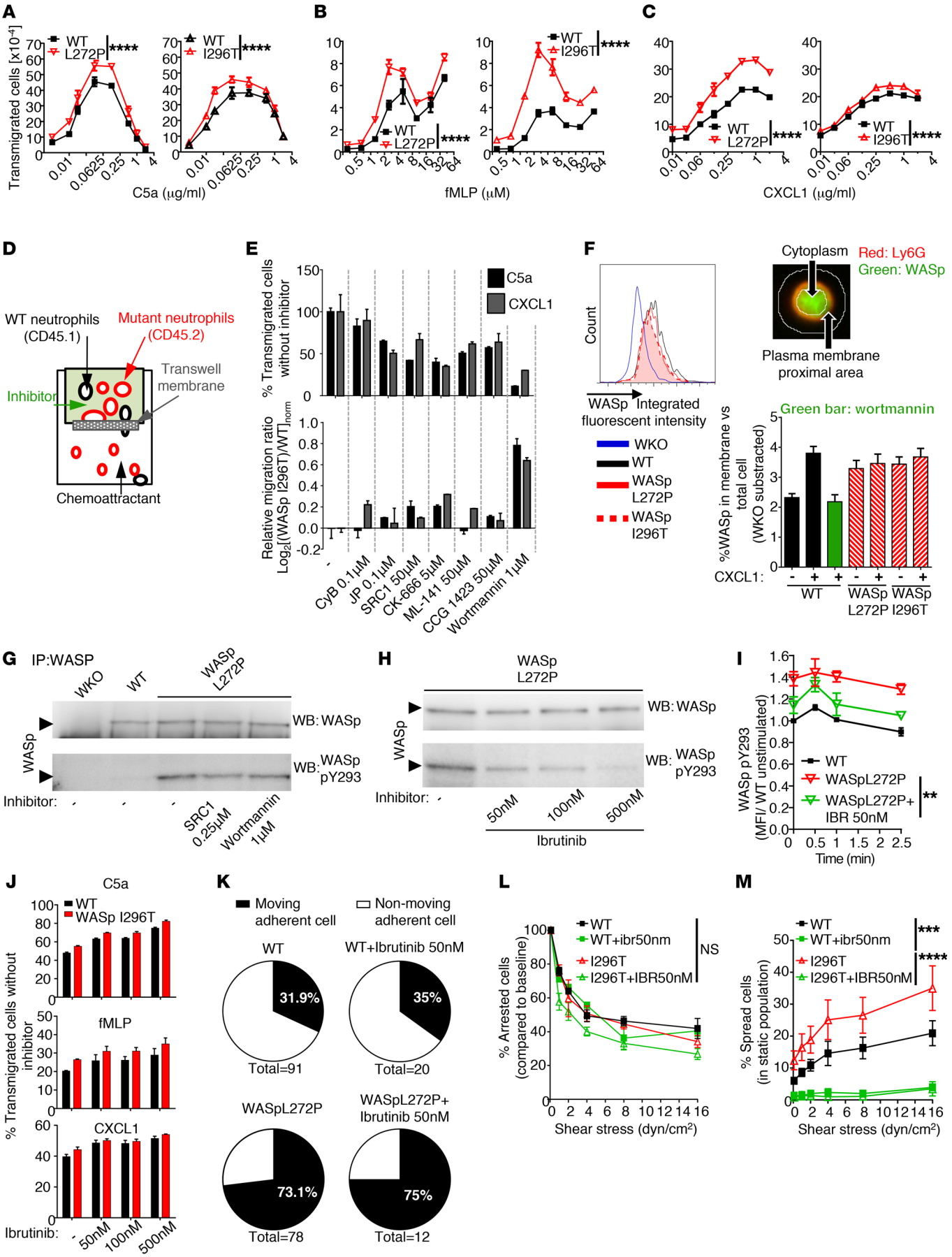
A
Transmigrated cells [x10⁻⁴]
WT
L272P
I296T
****
C5a (μg/ml)
B
fMLP (μM)
C
CXCL1 (μg/ml)
D
WT neutrophils (CD45.1)
Mutant neutrophils (CD45.2)
Transwell membrane
Inhibitor
Chemoattractant
E
% Transmigrated cells without inhibitor
C5a
CXCL1
Relative migration ratio Log2(WASp I296T/WT)norm
CyB 0.1μM
JP 0.1μM
SRC1 50μM
CK-666 5μM
ML-141 50μM
CCG 1423 50μM
Wortmannin 1μM
F
Count
WASp Integrated fluorescent intensity
WKO
WT
WASp L272P
WASp I296T
Cytoplasm
Red: Ly6G
Green: WASp
Plasma membrane proximal area
Green bar: wortmannin
%WASp in membrane vs total cell (WKO substracted)
CXCL1:
G
IP:WASP
WKO
WT
WASp L272P
WB: WASp
WB: WASp pY293
Inhibitor:
SRC1 0.25μM
Wortmannin 1μM
H
WASp L272P
Ibrutinib
50nM
100nM
500nM
I
WASp pY293 (MFI/ WT unstimulated)
WASpL272P
WASpL272P+ IBR 50nM
Time (min)
J
C5a
WASp I296T
% Transmigrated cells without inhibitor
fMLP
CXCL1
Ibrutinib:
K
Moving adherent cell
Non-moving adherent cell
WT
WT+Ibrutinib 50nM
31.9%
35%
Total=91
Total=20
WASpL272P
WASpL272P+ Ibrutinib 50nM
73.1%
75%
Total=78
Total=12
L
% Arrested cells (compared to baseline)
WT+ibr50nm
I296T
I296T+IBR50nM
NS
Shear stress (dyn/cm²)
M
% Spread cells (in static population)
***
****

Figure 6. Increased in vitro migration, membrane translocation, and Btk-dependent phosphorylation of WASp in XLN neutrophils. (**A**–**C**) Migration of WT vs. WASp L272P and WASp I296T bone marrow neutrophils toward the indicated chemoattractants in Transwell plates. Measured with flow cytometry. *n* = 3 replicates, *n* = 3 experiments/chemoattractant. (**D** and **E**) WT (CD45.1) and WASp XLN (CD45.2) neutrophils were mixed at a 1:1 ratio in the upper well of a Transwell plate and incubated for 10 minutes with inhibitors. Migration rate toward C5a or CXCL1 was plotted. *n* = 2 experiments. (**F**) WASp intracellular expression was measured by imaging flow cytometry. Ratios of plasma membrane proximal (determined by Ly6G surface staining) WASp and WASp in the total cell was plotted. Data are shown as mean + SEM of at least 198 neutrophils. *n* = 3 experiments. (**G**) WASp and phospho-Y293 WASp in SRC1- and Wortmannin-pretreated neutrophils were measured by Western blot. *n* = 2. (**H**) WASp and phospho-Y293 WASp in WASp L272P neutrophils before and after ibrutinib treatment. *n* = 3. (**I**) WASp Y293 phosphorylation upon CXCL1 activation with or without ibrutinib treatment (flow cytometry). *n* = 3. (**J**) Transwell migration of WT and WASp I296T neutrophils toward C5a (0.125 μg/ml), fMLP (3 μM), and CXCL1 (0.25 μg/ml) after incubation with ibrutinib. *n* = 3. (**K**) Ratio of motile cells among adherent cells on rmP-selectin, rmICAM-1, and rmCXCL-1 under flow as in Figure 5G. (**L**) Numbers of arrested cells as percentages of arrested cells at 0.1 dyn/cm^2 as in Figure 5E. (**M**) Ratio of spread cells at increasing flow rate as in Figure 5F. *n* = 3 replicates, *n* = 2 experiments. Data are represented as mean ± SEM. Two-way ANOVA was used for statistical significance. $^{**}P < 0.01$; $^{***}P < 0.001$; $^{****}P < 0.0001$.

tion of cellular F-actin, we used confocal microscopy and found increased F-actin in both the cortex and cytoplasm of XLN neutrophils (Figure 3F). Light microscopy and TEM analysis showed that bone marrow neutrophils from WASp L272P and WASp I296T mice had normal morphology (Supplemental Figure 3, M–O). To study surface topography, bone marrow neutrophils were examined using scanning electron microscopy. WASp L272P and WASp I296T neutrophils had an increased proportion of cells with highly ruffled surfaces when compared with WT neutrophils (Figure 3G). These data suggest that WASp L272P and WASp I296T exist in an open conformation that is spontaneously phosphorylated in the absence of stimuli. Moreover, WASp L272P and WASp I296T induce increased polymerized actin associated with altered surface topography of neutrophils.

Increased migration of WASp XLN neutrophils to the spleen and to the site of inflammation. To test the functional consequence of the WASp XLN mutation on neutrophil migration, we injected *Staphylococcus aureus* into mice by intradermal and i.p. injection and quantified infiltrated neutrophils at the injection sites. WASp L272P and WASp I296T mice had increased numbers of infiltrating neutrophils when compared with WT mice (Figure 4, A and B). To address the competitive fitness of WASp L272P and WASp I296T neutrophils side by side, we used mixed bone marrow chimeras. A mix of congenic CD45.1$^+$ WT and CD45.2$^+$ mutant bone marrow cells was injected into lethally irradiated hosts and analyzed 8 to 10 weeks after transfer. In the blood, WT, WASp L272P, and WASp I296T neutrophils showed similar ratios of cells when compared with the injected ratio of cells (Figure 4C). In contrast, WASp L272P and WASp I296T neutrophils showed a 2-fold competitive advantage over WT neutrophils in the bone marrow, spleen, and peritoneum upon thioglycollate-induced peritonitis (Figure 4C), suggesting that WASp XLN neutrophils accumulate in tissues.

We next considered the possibility that WASp L272P or WASp I296T neutrophils migrated more rapidly from the blood into tissues. We used a competitive setting in which a mix of bone marrow neutrophils expressing CD45.1 (WT) or CD45.2 (mutant) were injected i.v. into WT F1(CD45.1 × CD45.2) recipient mice. We applied the air pouch model to examine neutrophil extravasation and accumulation into an empty pocket of the skin. To attract neutrophils to extravasate through the endothelium, *N*-formyl-met-leu-phe (fMLP) and TNF-α were injected into the air pouch (Figure 4D). When compared with WT neutrophils, WASp L272P and WASp I296T neutrophils showed a competitive advantage in homing into the spleen and the air pouch (Figure 4D). In contrast, WASp-KO neutrophils had a selective disadvantage in homing into the spleen and the air pouch (Figure 4D). Together, these data suggest that WASp L272P and WASp I296T neutrophils migrated more rapidly from the blood and accumulated in the tissues.

Increased actin dynamics, spreading, and motility of WASp XLN neutrophils. WASp XLN neutrophils showed elevated total F-actin and WASp Y293 phosphorylation under static conditions. Neutrophil extravasation into tissues depends on coordinated changes in adhesion and migration (7). This process is synchronized by actin dynamics to form adhesive structures by the clustering of integrins such as CD11b and acts by forming vinculin-containing podosomes and leading edge lamellipodia with rapid actin polymerization and depolymerization. WT and WASp L272P and WASp I296T neutrophils formed CD11b clusters and podosomes on fibrinogen-coated surfaces (Supplemental Figure 4, A, D, and E). The lamellipodia of WASp L272P and WASp I296T neutrophils covered a smaller area when compared with WT neutrophils (Supplemental Figure 4F), and podosome numbers in WASp L272P, but not in WASp I296T, neutrophils were decreased (Supplemental Figure 4G). We next determined whether the increased cortical F-actin in XLN WASp neutrophils would lead to more dynamic changes in cell shape and adhesion. To evaluate actin polymerization in live cells, we crossed WT, WASp L272P, and WASp I296T mice with Lifeact-EGFP transgenic mice that express a fluorescently tagged peptide with high affinity to F-actin (28). Cellular morphology of neutrophils from WASp L272P × Lifeact-EGFP and WASp I296T × Lifeact-EGFP mice was monitored with imaging flow cytometry. Upon activation with PMA or fMLP, we found that neutrophils lost their circular shape and acquired an irregular shapes (Figure 5A). When compared with WT × Lifeact-EGFP cells upon fMLP activation, WASp L272P × Lifeact-GFP and WASp I296T × Lifeact-EGFP neutrophils showed a higher proportion of cells with irregular shape (Figure 5A).

To determine whether increased actin dynamics corresponded to increased WASp activation, we examined WASp Y293 phosphorylation by flow cytometry. The chemoattractant CXCL1 is produced by the activated endothelium to recruit neutrophils to the site of inflammation. When neutrophils were activated with CXCL1, WT neutrophils exhibited a rapid transient phosphorylation of WASp Y293, while the WASp XLN neutrophils showed a higher amplitude of phosphorylation that remained high during the 4 minutes monitored (Figure 5B). This was associated with higher amplitude of actin polymerization in CXCL1-stimulated WASp XLN neutrophils when compared with WT neutrophils (Figure 5C).

Integrin-mediated firm adhesion in postcapillary venules is actin mediated and dependent on WASp activity, as determined in WASp-KO neutrophils (29). To model neutrophil adhesion in blood vessels, we placed neutrophils into plastic flow chambers coated with recombinant P-selectin, ICAM-1, and CXCL1 molecules. Under a steady 2 dyn/cm^2 flow rate, WT neutrophils rolled on the substratum, arrested, and spread (Figure 5D). To test the hypothesis that increased in vivo migration was caused by increased integrin-mediated attachment, we compared the release rate of arrested cells and spread cells of WT and WASp XLN neutrophils under increasing shear stress by flow rate. WASp L272P and WASp I296T neutrophils had similar rates of release when compared with WT neutrophils (Figure 5E). However, the percentage of spread cells among all adherent cells (arrested and spread) was higher in WASp L272P and WASp I296T neutrophils (Figure 5F), showing increased adhesion of WASp XLN neutrophils under shear stress. Analysis of random motility of spread cells revealed that WASp XLN neutrophils showed significantly higher random movement, measured as displacement from the point of origin (Figure 5, G and H). Together, these data suggest that XLN neutrophils have a dynamic actin cytoskeleton, leading to increased spreading and increased movement of spread cells.

Increased membrane translocation and Btk-dependent phosphorylation of WASp in XLN neutrophils. We next determined whether increased actin dynamics and adhesion under flow would correspond to increased migratory response of WASp XLN neutrophils. To test this possibility, we examined neutrophil migration in vitro toward the neutrophil chemoattractants C5a, fMLP, and CXCL1. WASp L272P and WASp I296T neutrophils showed increased migratory response to C5a, fMLP, and CXCL1 when compared with WT neutrophils (Figure 6, A–C). To determine the mechanism of increased XLN neutrophil migration, we mixed WT (CD45.1) and WASp I296T (CD45.2) neutrophils and compared their migration rates toward C5a or CXCL1 with or without pretreating the cells with various inhibitors of intracellular signaling (Figure 6D). Inhibitors that targeted the actin cytoskeleton, Src kinases, or Cdc42 affected the migration of WT and WASp I296T neutrophils similarly (Figure 6E). In contrast, treating neutrophils with the PI3K inhibitor wortmannin gave WASp I296T neutrophils migratory advantage over WT neutrophils (Figure 6E). Importantly, low concentration of wortmannin gave migration advantage to WASp L272P and WASp I296T neutrophils (Supplemental Figure 5A).

Inhibition of PI3K by wortmannin affects the production and distribution of phosphatidylinositol derivatives in the plasma membrane. From biochemical studies, WASp may interact directly with one of these membrane derivatives, PIP2, via the WASp pleckstrin homology domain (19). To determine whether WASp XLN mutations affected plasma membrane localization of WASp, we used imaging flow cytometry and examined WASp localization in neutrophils. Upon CXCL1 activation, WASp was recruited from the cytoplasm to the plasma membrane in WT neutrophils (Figure 6F and Supplemental Figure 5B). WASp membrane translocation was inhibited by wortmannin, indicating that this process is PI3K dependent (Figure 6F). WASp L272P and WASp I296T were constitutively located proximal to the plasma membrane, even in the absence of CXCL1 stimulation (Figure 6F and Supplemental Figure 5B).

WASp XLN neutrophils were less sensitive to inhibition of PI3K in the Transwell competitive assay and exhibited increased adhesion under flow, which is a PI3K-dependent process (Supplemental Figure 5C). This effect was not due to increased PI3K signaling in WASp L272P and WASp I296T neutrophils, since phosphorylation of AKT, a main target of PI3K, was similar in unstimulated and stimulated WT and WASp XLN neutrophils (Supplemental Figure 5, D and E). To evaluate whether WASp activation depends on PI3K-induced signaling, we determined whether pharmacological inhibition of PI3K and also Src kinases would inhibit the spontaneous Y293 phosphorylation of WASp XLN. High concentration of wortmannin or Src1 inhibitors did not reduce WASp phosphorylation in WASp L272P neutrophils (Figure 6G and Supplemental Figure 5F). Based on studies of macrophages and neutrophils, Btk has been suggested as phosphorylating WASp (30, 31). The Btk inhibitor ibrutinib effectively reduced the spontaneous phosphorylation of Y293 in WASp L272P (Figure 6H and Supplemental Figure 5G). To determine whether ibrutinib could affect sustained phosphorylation of WASp XLN, we examined pWASp Y293 upon CXCL1 stimulation by flow cytometry. Ibrutinib treatment lowered the sustained hyperphosphorylation of WASp XLN (Figure 6I). To determine the functional consequence of ibrutinib treatment of WASp XLN neutrophils, we examined in vitro chemotaxis and cell spreading under shear stress. Ibrutinib treatment did not inhibit Transwell chemotaxis or the ratio of motile adherent cells and arrested cells under shear stress (Figure 6, J–L), but it markedly reduced the number of spread cells under shear stress of both WT and WASp XLN neutrophils (Figure 6M). Together, these data suggest that WASp is one of the targets of Btk for neutrophil spreading mediated by integrin activation, as previously shown (31). For cell movement, WASp activation occurs upstream of PI3K signaling and the L272P and I296T mutations render WASp less dependent on PI3K signalling.

Increased phagocytosis rate but normal killing of bacteria in XLN neutrophils. To consider host defense responses in XLN, we first examined in vitro killing of Gram-negative and Gram-positive bacteria by WASp XLN neutrophils. We found that the ability to kill *E. coli* or *S. aureus* was intact in WASp XLN neutrophils (Figure 7, A and B). We next examined the ability of neutrophils to phagocytose fluorescently labeled serum-opsonized *E. coli* and *S. aureus*. WASp L272P and WASp I296T neutrophils had a higher capacity to phagocytose bacteria when compared with WT neutrophils (Figure 7, C and D). Intracellular ROS production was similar between WT and WASp XLN neutrophils when incubated with heat-killed, opsonized *E. coli* or *S. aureus* and the cell-permeable luminol substrate (Figure 7, E and F). Intriguingly, when compared with WT neutrophils, WASp L272P and WASp I296T neutrophils had increased intracellular ROS production upon receptor-independent PMA activation (Figure 7G). The increased intracellular ROS production in WASp XLN neutrophils was also evident after quenching extracellular superoxide with superoxide dismutase (SOD) (Supplemental Figure 6A).

Extracellular ROS produced by translocation of NADPH components to the plasma membrane was measured with lucigenin. When compared with WT neutrophils, WASp L272P and WASp I296T neutrophils had reduced extracellular ROS production upon stimulation with *S. aureus,* fMLP, and PMA (Figure 7, H–J).

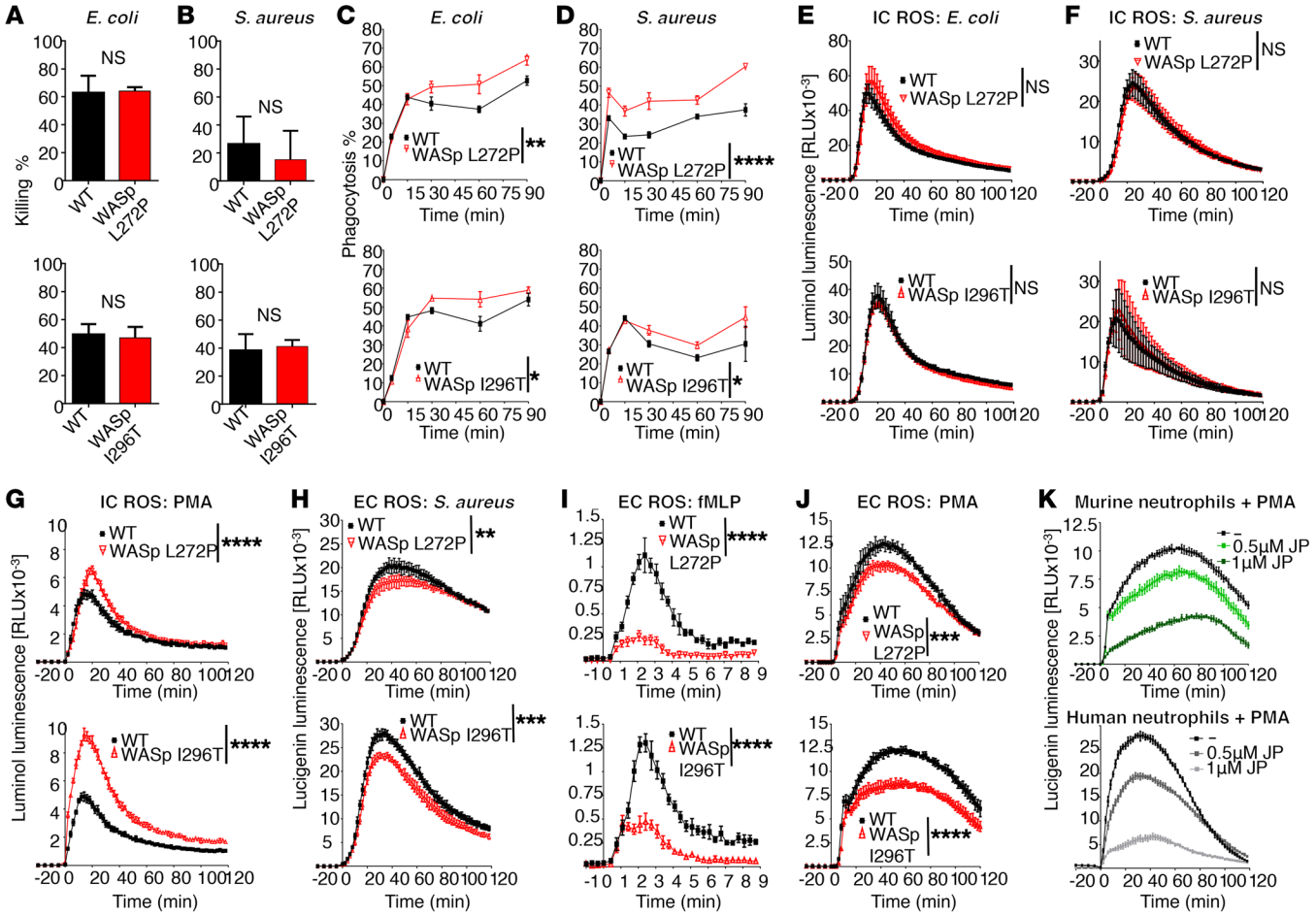

Figure 7. Increased phagocytosis rate, normal killing of bacteria, and dysregulated ROS responses in XLN neutrophils. *E. coli* (**A**) and *S.aureus* (**B**) killing capacity of WT and WASp XLN neutrophils were assessed by coincubating serum-opsonized bacteria and neutrophils at a ratio of 1:5 (*E. coli*/neutrophil) for 60 minutes (**A**) or 1:1 (*S.aureus*/neutrophil) for 60 and 90 minutes as shown in upper and lower panels, respectively (**B**). $n = 3$ replicates, $n = 3$ experiments with each bacteria. (**C** and **D**) Phagocytosis of Alexa Fluor 488–labeled, serum-opsonized *E. coli* (**C**) and *S. aureus* (**D**) by WT WASp XLN neutrophils measured by flow cytometry. $n = 3$ replicates, $n = 3$ experiments with each bacteria. (**E**–**G**) Intracellular ROS (IC ROS) measured with luminol chemiluminescence in murine bone marrow neutrophils upon stimulation with *E. coli* ($n = 8$) (**E**), *S.aureus* ($n = 10$) (**F**), or PMA ($n = 18$). $n = 4$. Data are shown as mean ± SD, 2-way ANOVA. (**H**–**J**) Extracellular ROS (EC ROS) was measured using a lucigenin chemiluminescence assay in murine bone marrow neutrophils upon stimulation with (**H**) heat-killed serum-opsonized *S. aureus* ($n = 18$), (**I**) fMLP ($n = 4$), or (**J**) PMA ($n = 26$). $n = 4$. Data are shown as mean ± SD. Two-way ANOVA. (**K**) Extracellular ROS was measured upon PMA stimulation of murine (upper panel) and human healthy donor (lower panel) neutrophils with or without pretreatment with jasplakinolide. $n = 5$. Data are shown as mean ± SD. $^*P < 0.05$; $^{**}P < 0.01$; $^{***}P < 0.001$; $^{****}P < 0.0001$.

To determine whether increased cortical F-actin in XLN neutrophils impaired extracellular ROS production, we treated control human and WT murine neutrophils with the actin-stabilizing drug jasplakinolide. Upon treatment with jasplakinolide and PMA activation, both human and murine WT neutrophils had lower extracellular ROS production (Figure 7K).

Altered granule release in XLN neutrophils. We reasoned that changes in intra- and extracellular ROS may be a result of altered trafficking of granules to the surface. To test this hypothesis, we measured secretion of neutrophil elastase that, together with other serine proteases, such as proteinase 3 and cathepsin G, is stored in large quantities in azurophilic granules (32). We used a probe that emits fluorescence upon cleavage by neutrophil elastase. WT and XLN murine neutrophils showed low secretion of elastase in response to fMLP (Figure 8A). Upon treatment of neutrophils with cytochalasin B to depolymerize the cortical actin cytoskeleton, XLN neutrophils showed higher elastase secretion when compared with WT neutrophils in both the presence and absence of fMLP (Figure 8A and Supplemental Figure 7A). Importantly, secretion of CD11b that is present in specific granules, gelatinase granules, and secretory vesicles (32) does not require cytochalasin priming. To investigate the effect of WASp L272P and WASp I296T on CD11b distribution in neutrophils, we activated neutrophils with PMA. Upon activation, WT neutrophils upregulated CD11b on their cell surface. When compared with WT bone marrow and blood neutrophils, CD11b surface expression was lower on WASp L272P and WASp I296T neutrophils upon activation (Figure 8, B and C, and Supplemental Figure 7, B and C). The upregulation of CD11b was also lower in WASp L272P and WASp I296T neutrophils upon stimulation with the neutrophil chemoattractant C5a (Figure 8D), whereas shedding/internalization of the C5a receptor (C5aR) was similar in WT and XLN neutrophils (Supplemental

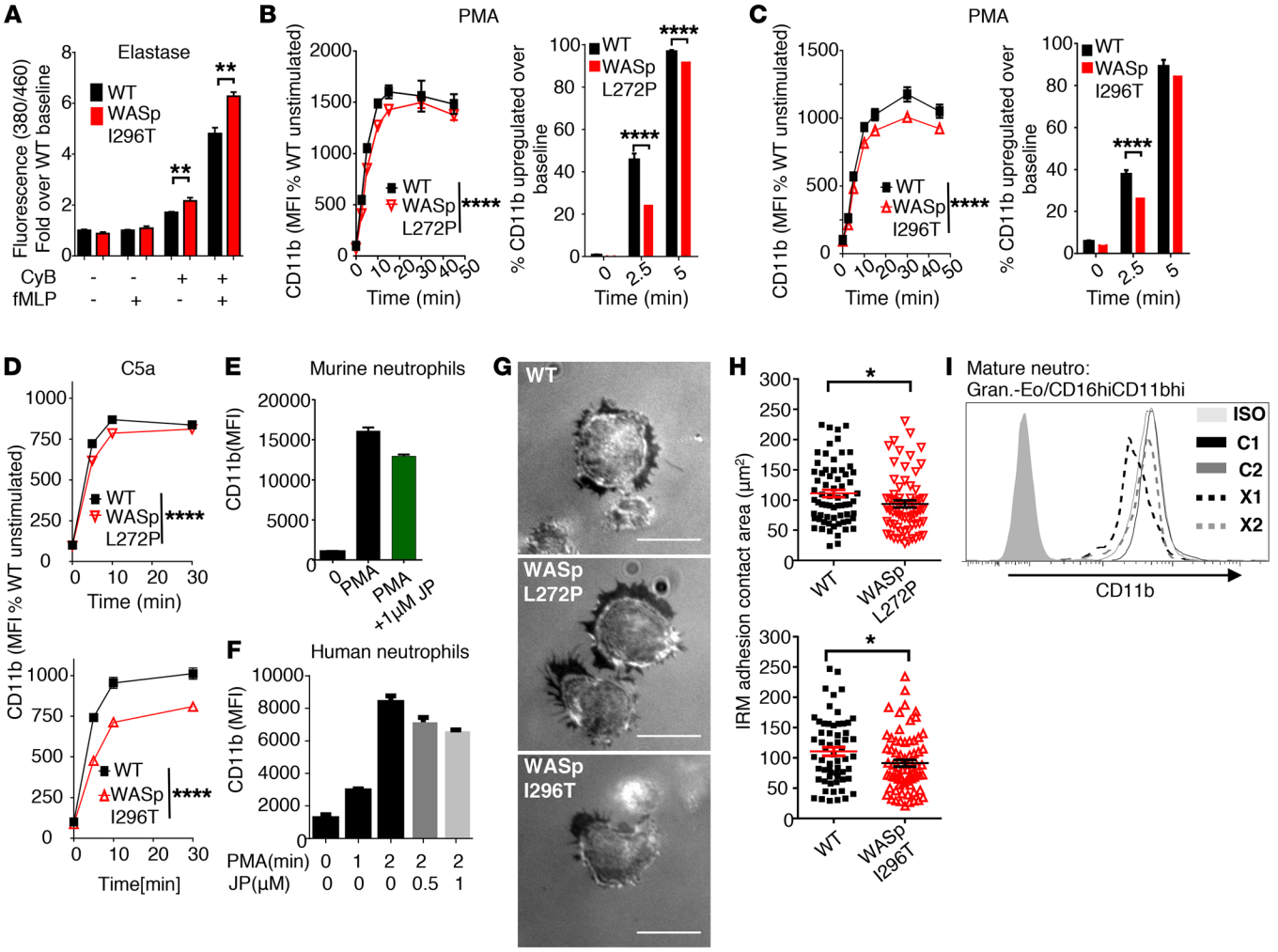

Figure 8. Altered granule release in XLN neutrophils. (**A**) Neutrophil elastase secretion by WT and WASp I296T neutrophils was measured with fluorescent detection of the cleavage of MeOSuc-AAPV-AMC substrate after 90 minutes of activation with 10 μM fMLP in the presence of 5 μg/ml cytochalasin B (CyB). *n* = 4 replicates, *n* = 3 experiments. (**B** and **C**) Upregulation of CD11b upon activation of bone marrow–derived neutrophils with PMA (left panels). Data are represented as percentage of WT unstimulated signal. Percentage of cells above arbitrary baseline MFI of CD11b (right panels). Bonferroni's corrected *t* test. *n* = 4 replicates, *n* = 4 experiments. (**D**) CD11b expression of bone marrow–derived neutrophils upon C5a stimulation. Two-way ANOVA. *n* = 3. (**E** and **F**) CD11b expression on PMA-activated murine (**E**) and human (**F**) neutrophils. When indicated, neutrophils were preincubated for 30 minutes with jasplakinolide. *n* = 3 (murine); *n* = 2 (human). (**G**) Interference reflection microscopy (IRM) images of 5-minute fMLP-activated, adherent neutrophils on fibrinogen-coated glass. Scale bars: 10 μm. (**H**) Quantification of adhesion contact area on interference reflection microscopy images. Minimum count of 14 fields per genotype. Mann-Whitney *U* test. *n* = 4 experiments. (**I**) CD11b expression on mature neutrophils (granulocytes-eosinophils/CD16HICD11bHI) from WASp L270P XLN patients (X1, X2) and 2 healthy male controls (C1, C2) analyzed by flow cytometry. Unless otherwise indicated, data are represented as mean ± SEM. One-way (**A**) or 2-way ANOVA (**B**–**D**) was used to test statistical significance. **P* < 0.05; ***P* < 0.01; *****P* < 0.0001.

Figure 7D). The total pool of surface plus intracellular CD11b was similar between WT and WASp XLN neutrophils (Supplemental Figure 7, E and F), suggesting that decreased surface expression of CD11b in XLN neutrophils was caused by reduced trafficking of CD11b from intracellular vesicles to the cell surface. To determine whether increased cortical F-actin in XLN neutrophils impaired translocation of CD11b to the cell surface, we treated control WT murine and human neutrophils with the actin-stabilizing drug jasplakinolide. Upon treatment with jasplakinolide and PMA activation, both murine WT and human neutrophils had lower expression of CD11b (Figure 8, E and F). In contrast to XLN neutrophils, WASp-KO neutrophils had decreased cortical F-actin (Supplemental Figure 7, G and H) and showed increased CD11b cell-surface expression upon PMA activation (Supplemental Figure 5I). Our mixed bone marrow chimera experiment (Supplemental Figure 7J) provided the possibility of examining CD11b expression in WT and XLN neutrophils side by side. When compared with WT neutrophils in the same chimera mouse, WASp L272P and WASp I296T neutrophils in the bone marrow, blood, and spleen had lower surface expression of CD11b (Supplemental Figure 7J).

To examine the functional consequence of decreased surface CD11b, we used internal reflection microscopy (IRM) to examine the adhesive surface of neutrophils toward fibrinogen-coated glass at steady state. When compared with WT neutrophils, WASp L272P and WASp I296T neutrophils had smaller adhesive surface area, suggesting reduced integrin-mediated firm adhesion (Fig-

ure 8, G and H). The decrease of lamellopodia size (Supplemental Figure 4F) was proportional to the decreased adhesion footprint (Supplemental Figure 7K).

We next examined CD11b surface expression of neutrophils from the XLN patients. We found that CD11b expression was reduced on XLN neutrophils when compared with C1 and C2 control cells (Figure 8I).

Together, these data show that, despite reduced myelopoiesis in XLN, the increased activity of WASp compensated for this dysfunction by WASp localization to the plasma membrane in a constitutively active state that induced increased actin dynamics and elevated neutrophil adhesion and migration.

Discussion

Studies of WASp-deficient neutrophils have revealed the importance of WASp for neutrophil migration and function (29, 31). We reasoned that XLN mutations in WASp may affect multiple steps during neutrophil development in bone marrow and effector functions in tissues. We took a translational approach and combined analysis of neutrophils in XLN patients with 2 XLN mouse models that we generated. We found evidence for paucity in myelopoiesis in XLN patients and also that the few neutrophils present in peripheral blood showed a hyperactivated phenotype. Interestingly, XLN patients had normal numbers of neutrophils in saliva, indicating the presence of neutrophils at peripheral sites, such as the periodontal tissue. Using the XLN mouse models, we found that XLN neutrophils displayed increased chemokine-induced migration and integrin-mediated adhesion under flow and that they accumulated in tissues. We provide molecular evidence in primary neutrophils showing that the hyperactivity of XLN neutrophils is caused by constitutive phosphorylation of the critical residue WASp Y293, WASp localization proximal to the plasma membrane, and exposure of the WASp VCA domain that induces actin polymerization even in the absence of receptor stimulation. Our data show that regulated WASp activity regulated by conformation change is required for coordinating cellular signaling to actin dynamics in neutrophils.

We studied human peripheral blood and saliva from 2 WASp L270P XLN patients (16) and control subjects. As expected (16), blood neutrophil numbers were extremely low in the XLN patients. The XLN patient neutrophils had an activated phenotype, as evidenced by elevated surface expression of gp91 and degranulated morphology. Despite the low blood count in XLN patients, the number of neutrophils in their saliva was normal, suggesting that neutrophils accumulated in tissues. Importantly, this notion is supported by the relatively mild clinical symptoms of XLN patients compared with those with other types of SCNs. Beel et al. described patients with the WASp I294T mutation as having considerable variation in infectious history, and the severity of their neutropenia did not correlate closely with their susceptibility to infections (15). Ancliff and colleagues reported that a patient with WASp S272P mutation has less severe phenotype than classic SCN and that the patient responded well to more modest doses of G-CSF (17). Moreover, no gingivitis or periodontitis has been detected in XLN patients, although this is one of the cardinal clinical symptoms of other SCNs (1–3). Our data together with the clinical findings suggest that the granulocyte compartment in XLN patients compensates for the partial myeloid differentiation blockade in the bone marrow. Moreover, the extremely low absolute neutrophil number in blood does not reflect the effector potential of the neutrophil pool.

To understand the pathophysiology of XLN and how activating mutations in WASp affects neutrophils, we generated 2 independent knockin mouse models harboring the corresponding murine XLN mutations WASp L272P and WASp I296T. We followed our XLN mouse colonies until 12 months of age and found no signs of low neutrophil numbers in peripheral blood or any neutrophil-related illness. Neither did we detect any signs of bone marrow failure upon G-CSF administration in XLN mice. Many attempts have been made to generate mouse models for human neutrophil deficiency. Some mouse models show neutropenia, including those lacking G6PC3 or Rac2 (33, 34), but in other mouse models, such as those lacking neutrophil elastase, neutropenia fails to develop (35). It is possible that mouse models fail to capture certain aspects of SCN, such as progressive bone marrow failure. Furthermore, penetrance of neutropenia in male carriers of XLN mutation is incomplete, which highlights the possibility of epistatic genetic interaction between WASp and other unknown gene variants or environmental effects in XLN pathogenesis that may not be recapitulated in our inbred C57BL/6 mouse model. Notably, our mice were kept under specific pathogen–free (SPF) conditions, which results in a relatively low homeostatic blood neutrophil number, which also occurs in WT mice (36–38). We show that XLN patients had a reduced plasma level of the antimicrobial peptide hCAP18, which is produced during early myelopoiesis, and that WASp L270P $CD34^+$ stem cells and progenitors matured into neutrophils at a reduced rate in vitro. This result suggests a partial developmental defect in bone marrow (25, 26).

The amino acid sequences of murine and human WASp are 86% identical and the GBD domains are 100% identical. Despite the apparent failure of the 2 WASp XLN mouse strains to model aberrant myeloid differentiation, we reasoned that the XLN mouse models are superior to human blood samples for investigating WASp XLN neutrophils in vitro. We showed that the extremely low numbers of granulocytes detected by flow cytometry in human blood or purified by density gradient centrifugation were heavily enriched for eosinophils. This enrichment of eosinophils may bias the interpretation of clinical assays aimed at studying neutrophils in blood samples. We found in primary murine neutrophils that WT WASp was present in protein lysates, whereas the WASp XLN protein rapidly underwent proteolytic degradation. The degradation of WASp XLN could be prevented by pretreatment with a potent serine protease inhibitor. This suggests that WT WASp was protected from neutrophil proteases during cell lysis, whereas WASp XLN was rapidly degraded when exposed to neutrophil proteases because of its open conformation. Consistent with our data from studies of murine XLN B and T cells with increased loads of F-actin (39), WASp XLN mutations caused spontaneous actin polymerization in neutrophils both in the cytoplasm and in the cortical F-actin network. This shows that the VCA domain of WASp XLN is constantly exposed for binding to the Arp2/3 complex, leading to actin polymerization. From studies of N-WASp using in vitro systems (19), it has been suggested that WASp in the open conformation may be recruited to membranes by interaction with PIP2. We found that WASp XLN localized proximally to the plasma membrane in primary neutrophils, even in the

absence of stimuli. Another predicted consequence of WASp in open conformation was increased phosphorylation of WASp. When the autoinhibition of WASp is released by Cdc42 and PIP2, the critical Y291 (Y293 in mouse) is exposed and phosphorylated, allowing for binding to kinases that prolong the activated, open conformation state of WASp in the absence of Cdc42 (21). We show in primary neutrophils that Y293 was hyperphosphorylated in WASp L272P and WASp I296T, even in the absence of stimuli. High basal L270P phosphorylation has been found previously in COS-7 cells transfected with WASp L270P (40). Interestingly, the phenotype of WASp XLN partially overlaps with that of the phosphomimicking mutant WASp Y293E (41). The WASp Y293E mutant induces increased actin polymerization in vitro, and the WASp Y293E protein was degraded in protein lysates (41).

Surprisingly, we found that WASp XLN neutrophils migrated to tissues at an increased rate using 4 different models: *S. aureus*–induced peritonitis and dermatitis, thioglycolate-induced sterile peritonitis in mixed bone marrow chimeras, and competitive homing experiments. Neutrophil migration into tissue requires active regulation of the actin cytoskeleton. First, neutrophil extravasation requires actin-mediated spreading on the activated endothelium, which is regulated by integrin outside-in signaling. Second, amoeboid migration requires a coordinated regulation of actin polymerization in pseudopodia and retraction of uropods. Here, we show that a high proportion of WASp XLN neutrophils acquired an irregularly shaped cortical actin upon activation, indicating enhanced actin dynamics. CXCL1 activation of neutrophils caused a rapid transient phosphorylation of WASp Y293, which was more prolonged and had higher amplitude in WASp XLN neutrophils. These increased actin dynamics in WASp XLN neutrophils can be directly connected to the increased rate of extravasation in flow chamber assays, for which we showed an increased rate of adhesion of WASp XLN neutrophils to β_2 integrin ligand–coated (ICAM-1) surface upon activation with P-selectin and CXCL-1. The increased actin dynamics could also be detected using Transwell assays in which WASp XLN neutrophils showed increased migration toward C5a, fMLP, and CXCL1 gradients. In Transwell assays, WT and WASp XLN neutrophils were equally sensitive to F-actin–stabilizing (jasplakinolide) or –disrupting (cytochalasin B, CK-666) drugs, indicating that the dynamics and localization of the actin polymerization gives an advantage to WASp XLN neutrophils. Intriguingly, these neutrophils were also similarly sensitive to Cdc42 inhibition (ML-141), suggesting that WASp XLN migration is dependent on Cdc42. Finally, WASp XLN neutrophils were less sensitive to the migration-inhibiting effect of the PI3K inhibitor wortmannin. Activation-induced relocation of WASp to the plasma membrane was also PI3K dependent, and we speculate that WASp relocation and migration are connected. Recent work of Zarbock and colleagues (42) shows that WASp in neutrophils can be recruited to the plasma membrane via Skap2, which binds PIP3, providing a possible mechanism of wortmannin sensitivity. Finally, by pharmacological inhibition, we found that the hyperphosphorylation of WASp XLN was dependent on Btk, suggesting that WASp is a direct target of Btk.

To address whether WASp is involved in regulating host defense properties of neutrophils, we tested bacteria killing, phagocytosis, and ROS production. WT and WASp XLN neutrophils had similar capacities for killing *S. aureus* and *E. coli* in vitro. To further dissect the interaction between neutrophils and bacteria, we measured the uptake of opsonized *S. aureus* and *E. coli*. Consistent with increased actin dynamics, WASp XLN neutrophils had enhanced capacities to phagocytose opsonized Gram-positive and Gram-negative bacteria. *S. aureus*– and *E. coli*–mediated intracellular ROS was similar between WT and WASp XLN neutrophils; however, receptor-independent intracellular ROS production was increased in WASp XLN neutrophils, indicating enhanced intracellular signalling. In contrast to intracellular ROS production, extracellular ROS production was defective in WASp XLN neutrophils when measured after either fMLP, PMA, or *S. aureus* stimulation. Since decreased extracellular ROS could be caused by reduced capacity to release intracellular vesicles by WASp XLN neutrophils, we examined surface translocation of CD11b. CD11b surface expression on murine and patient XLN neutrophils was lower than on control neutrophils at steady state and upon stimulation. We could mimic the phenotype of XLN neutrophils by pharmacological stabilization of F-actin using jasplakinolide, and we postulate that extracellular ROS and CD11b surface expression negatively correlates with the F-actin content of neutrophils. Severely reduced CD11b expression causes LAD-I (11). Our study suggests that increased actin dynamics with a hypermigratory response of neutrophils may be associated with moderately lower CD11b expression. The speed of cell migration is a function of attachment strength between the cell and the substratum, with maximal migration speed at an intermediate level of cell-substratum adhesiveness (43). Since migration requires cell detachment, we speculate that a small decrease in CD11b expression may lead to increased cell migration.

Our data show the importance of fine-tuning WASp activity by structural conformation, membrane localization, and tyrosine phosphorylation for normal neutrophil responses. We favor a model suggested by Rosen et al. (21) in which WASp in the open conformation is tyrosine phosphorylated by kinases, thus providing a molecular memory of WASp activation leading to actin polymerization. The XLN mutations expose the WASp Y293 residue that can be phosphorylated by kinases such as Btk, as we show here. This will lead to sustained WASp activity and the possibility of inducing WASp activity further, as indicated by our data. We show that WASp Y293 phosphorylation and actin polymerization could be induced in chemokine-stimulated XLN neutrophils, suggesting that WASp XLN can have induced activity. Moreover, we show increased motility of spread cells upon CD11b activation, suggesting increased dynamics of the actin cytoskeleton upon receptor activation and a dynamic contact area on an adhesive surface. The molecular memory model (21), together with our findings from investigation of XLN neutrophils, suggests that receptor activation can further enhance the amplitude of WASp activity inside a cell.

Although severe neutrophil defects have been shown in KO models of WAS, the contribution of these defects to disease pathogenesis is confounded by the profound immune dysregulation in other immune cell compartments. In contrast to WAS patients, XLN patients exhibit a clinical pathogenesis that largely appears as low neutrophil numbers in blood. Combining what is known of the relatively mild clinical presentation of XLN patients and the results of our study, we propose that XLN neutrophils can compensate for reduced bone marrow output by increased migration into tissues where they are functional. It is possible that increased

rates of adhesion by XLN neutrophils in vasculature contribute to relative neutropenia as measured in blood. Our study categorizes XLN as an atypical SCN in which low absolute neutrophil count in blood samples does not warrant life-long G-CSF support.

Methods

Patients. We analyzed peripheral blood and saliva from 2 XLN patients, 1 carrier female, 1 related female with unknown carrier status, and 3 healthy volunteers. Peripheral blood was anticoagulated on potassium EDTA or sodium heparin.

Mice. The WASp L272P and WASp I296T knockin strains were generated by inGenious Targeting Laboratory by insertion of a point mutation into germline *WASp* exon 9: TTG to CCG to generate the Leu-272 to Pro-272 knockin mutation or ATT to ACT to generate the Iso-296 to Thr-296 knockin mutation. WASp-L272P mice (C57BL/6 ES cells, C57BL/6 background) and WASp-I296T mice (mixed 129Sv and C57BL/6 ES cells, backcrossed for more than 7 generations to C57BL/6 background), WKO mice (mixed 129Sv and C57BL/6 ES cells, backcrossed at least 9 generations to C57BL/6 background) (44), and littermate WT controls were bred and maintained at the animal facility of the Department of Microbiology, Tumor and Cell Biology at Karolinska Institutet under SPF conditions. The Lifeact-EGFP transgenic mice (28) were originally obtained from Roland Wedlich-Söldner (University of Münster, Münster, Germany) and were crossed into WASp-L272P mice and WASp-I296T mice. Male mice were used at 6 to 12 weeks of age.

Neutrophil differentiation of human CD34⁺ progenitors. $CD34^+$ cells were purified from peripheral blood mononuclear cells with magnetic bead–positive selection (Miltenyi Biotec) and cultured with IL-3, SCF, and G-CSF for 13 days (45).

Neutrophils. Murine bone marrow neutrophils were isolated as described in Mócsai et al. (46). Briefly, bone marrow from femur and tibia was flushed and red blood cells were lysed with hypotonic salt solution. Bone marrow cell suspension was purified with 62.5 % density discontinuous Percoll (GE Healthcare Life Sciences) gradient centrifugation. The neutrophil-containing fraction contained over 85% neutrophil granulocytes. When higher purity was needed, neutrophils were isolated with magnetic bead–negative selection (Miltenyi Biotec). Human neutrophils were purified according to Nauseef et al. (27) with dextran sedimentation and Ficoll-Hypaque density gradient centrifugation.

Bone marrow chimera. For generation of mixed bone marrow chimeras, 1×10^7 total bone marrow cells, including WASp L272P or WASp I296T bone marrow cells (expressing CD45.2) and WT bone marrow cells (expressing CD45.1) at a 3:1 ratio, were transplanted via i.v. injection into lethally irradiated (13 Gy) WT C57BL/6 recipient animals.

In vivo homing experiments. The air pouch was created in F1(CD45.1 × CD45.2) mice by repeatedly injecting sterile air subcutaneously. At day 6 after initial injection, 1×10^7 WT (CD45.1) and WASp L272P, WASp I296T, or WKO neutrophils were injected at a 1:1 ratio i.v. into the F1(CD45.1 × CD45.2) recipients. Five hours after fMLP and TNF-α injection into the air pouch, mice were sacrificed and blood, bone marrow, spleen, and lavage from the air pouch were analyzed by flow cytometry. Grafted neutrophils (CD45.1 or CD45.2 single positive) were counted, and the following normalized and log-transformed values were plotted: $\log_2[\mathrm{Mut/WT}]_{\mathrm{norm}} = \log_2[(\mathrm{Mut/WT})/(\mathrm{Mut/WT})_{\mathrm{grafted}}] - \mathrm{Avg}(\log_2[(\mathrm{WT}_{\mathrm{CD45.2}}/\mathrm{WT}_{\mathrm{CD45.1}})/(\mathrm{WT}_{\mathrm{CD45.2}}/\mathrm{WT}_{\mathrm{CD45.1}})_{\mathrm{grafted}}])$, where Avg indicates average and Mut indicates mutant. The first logarithmic part in the equation represents the normalized migration ratio of mutant neutrophils compared with WT neutrophils (normalized to the original grafted ratio, quantified each time before the experiment) and the second average $\log_2$ value represents the migration bias caused by the CD45.1/.2 isoforms as determined in WT neutrophils.

ROS. Neutrophils (5×10^5) in HBSS/5% FCS were incubated in 96-well white flat-bottom plates (Thermo Fisher Scientific) for 30 minutes at 37°C with Luminol (Sigma-Aldrich; at 56 μM final concentration) or Lucigenin (Sigma-Aldrich; at 50 μM final concentration). ROS-induced chemiluminescent signals were measured with a luminometer (BMG Labtech) upon activation of the neutrophils with fMLP (final, 3 μM), PMA (final, 100 ng/ml), or heat-killed serum-opsonized *S. aureus* (1 neutrophil:10 bacteria).

Phagocytosis. Bone marrow–derived neutrophils and serum-opsonized A488-labeled *E. coli* or *S. aureus* (Thermo Fischer Scientific) were coincubated at a ratio of 1:5 at 37°C. Samples were taken at various time points, and the phagocytosis rate of bacteria was measured by flow cytometry.

In vitro killing of bacteria. Mouse serum–opsonized *E. coli* (WA321; DSMZ collection) or *S. aureus* (Seattle 1945; DSMZ collection) was incubated in a rotating tube at 37°C with neutrophils for the indicated time, and the ratio of neutrophils to bacteria after incubation was determined. Neutrophils were lysed in hypotonic solution, which was DNase I (Roche) digested and spread at various dilutions on Luria-Bertani or blood agar plates. CFUs were enumerated after 12 hours of incubation on plates at 37°C. Percentage of CFU decrease in neutrophil-bacteria mixtures was compared with bacteria without neutrophils.

Transwell migration assay. Bone marrow neutrophils in HBSS/5% FCS were added to the upper chambers of Transwells (3.0 μm pore size) (Costar). The lower chambers were filled with HBSS, 5% FBS, and concentrations of C5a, CXCL1, and fMLP as indicated in Figure 6. Plates were incubated for 2 hours at 37°C, and the number of transmigrated cells was measured by flow cytometry.

Flow cytometry. Single-cell suspensions were immunolabeled with the following antibodies after blocking nonspecific binding with CD16/32 (clone 93) (mouse) or human BD Fc block (BD Biosciences — Pharmingen) and 20% rabbit serum (all from Biolegend unless otherwise indicated): CD15 (clone W6D3), CD16 (clone 3G8), gp91phox (clone 7D5; LSBio), CD11b (clone M1/70), Siglec-8 (clone 7C9), CD45 (clone HI30), Ly6G (clone 1A8), C5aR (clone 20/70), CD45.1 (clone A20), CD45.2 (clone 104). DAPI staining was used to exclude dead cells. Cells were acquired with LSR Fortessa (BD) or ImageStream^X Mark II Imaging Flow Cytometer (Amnis). Analyses were completed using FlowJo software (TreeStar Inc.) and IDEAS v.6 software (Amnis).

Western blot. Neutrophils were lysed in Triton X-100 lysis buffer after a 10-minute preincubation of cells with the serine protease inhibitor diisopropylfluorophosphate (DPF) (5 mM, Sigma-Aldrich). Murine neutrophil protein lysates or immunoprecipitated lysates were run with 4% to 12% SDS-PAGE gel electrophoresis in MES buffer under reducing conditions using the Bolt Gel System (Thermo Fisher Scientific). Blots were developed with anti-WASp (Santa Cruz Biotechnology Inc.; B-9 and F-8 antibodies) and anti-WASp phospho-Y293 (Abcam).

Human hCAP18 was detected in plasma as described previously (26).

Light microscopy. For phalloidin and CD11b staining, bone marrow–derived neutrophils in cell suspension or adherent on fibrinogen were fixed (PFA Fixation Buffer, BioLegend), washed,

and permeabilized (BioLegend). Cells were stained with an Alexa Fluor 488– or Alexa Fluor 647–labeled phalloidin (Thermo Fisher Scientific) and CD11b (clone M1/70, BioLegend). Labeled cells were stained with secondary anti-rat Alexa Fluor 555 antibody (Thermo Fisher Scientific) and mounted on glass coverslips in Vectashield mounting medium with DAPI (Vector Laboratories). Slides were imaged using a Leica TCS SP5 confocal microscope or Leica DMRE (Leica). Analysis of cortical actin was performed using Fiji software (47).

Electron microscopy. For TEM, cells were fixed in 2.5% glutaraldehyde in 0.1 M phosphate buffer, pH 7.4, then postfixed in 2% osmium tetroxide (TAAB). After embedding in LX-112 (Ladd), ultrathin sections (approximately 50–60 nm) were cut and contrasted with uranyl acetate followed by lead citrate and examined in a Hitachi HT 7700 election microscope at 80 kV. Digital images were taken with a Veleta camera (Olympus Soft Imaging Solutions GmbH).

For scanning electron microscopy, specimens were fixed by immersion in 2.5% glutaraldehyde in 0.1 M phosphate buffer (pH 7.4), dried, and coated with 10 nm platinum (Q150T ES). The specimens were analyzed in an Ultra 55 field emission scanning electron microscope (Zeiss) at 3 kV.

Saliva. Saliva was extensively washed, stained with fluorescent antibodies, fixed with paraformaldehyde, and successively filtered through 70, 40, 20, and 10 μm filters.

Cytospin and staining. Cytospin (Shandon Scientific Co.) slides were stained with Differential Quik Stain (Polysciences Inc.) according to the manufacturer's protocol.

Flow chamber. μ-Slide $I^{0.4}$ (IBIDI GmbH) plastic flow chambers were coated with rmP-selectin (BioLegend), rmICAM-1 (R&D Systems), and rmCXCL-1 (BioLegend). Coated plastic flow chambers were perfused with bone marrow neutrophils at 0.1 dyn/cm^2, and shear stress was stepwise increased to indicated values every 30 seconds using a syringe pump (Chemyx Inc.). Images were taken with a Zeiss Axio Observer Z1 microscope (Zeiss).

Statistics. Analyses for statistical significance ($P < 0.05$) with 2-tailed Student's *t* test, 1-way ANOVA with post hoc Bonferroni's correction, or 2-way ANOVA, as indicated for the specific experiments, were performed with GraphPad Prism (GraphPad Software Inc.). Error bars represent SEM or, in ROS experiments, SD.

Study approval. The study was approved by the Institutional Review Board of University Hospitals Leuven, and all individuals gave written, informed consent. All animal experiments were performed after approval from the local ethical committee (the north Stockholm district court, permits N77/13 and N272/14).

Author contributions

MK and LSW designed the research. MK, JR, JSK, HW, CG, MT, PD, HB, LK, JJ, MH, MAPB, CIMD, AB, and KP performed the experiments and analyzed the data. SL and DPL supervised imaging flow cytometry analysis. WS supervised imaging analysis. PV provided XLN patient samples and analyzed patient data. SBS and LSW designed and generated the XLN mouse models. MK and LSW wrote the manuscript. All authors edited the manuscript.

Acknowledgments

The authors are grateful to the XLN patients and their families for supporting our study. We would like to thank Nancy Boeck and Sanne Smits at University Hospitals Leuven, Anne van der Does and Lennart Lindbom at Karolinska Institutet, and Siobhan Burns and Adrian Thrasher at University College London for valuable comments and/or technical instructions. We are grateful to the staff of the Department of Microbiology, Tumor and Cell Biology animal facility for their technical support and Kjell Hultenby for the electron microscopy. This work was supported by a postdoctoral fellowship from the Cancer Society (to MK), a postdoctoral fellowship from the Childhood Cancer Society (to JR), a clinical postdoctoral fellowship from the Swedish Society of Medical Research (to HB), a postdoctoral fellowship from Olle Engqvist Byggmästare (to MH), and a PhD fellowship from Fundação para a Ciência e a Tecnologia (SFRH/BD/47926/2008 to MAPB) as well as the OE and Edla Johanssons Foundation, the Lars Hierta Memorial Foundation, the Tore Nilsson Foundation (to MK), the Grochinsky Foundation (to HB), the Swedish Medical Society (to HB and LSW), the Swedish Research Council, the Cancer Society, the Childhood Cancer Society, the European Commission 7th framework Program Marie Curie (reintegration grant 249177), the Åke Olsson Foundation, the Jeansson Foundation, the Groschinsky Foundation, the Åke Wiberg Foundation, the Bergvall Foundation, King Gustaf V's 80-year Foundation, and the Karolinska Institutet (to LSW). LSW is a Ragnar Söderberg fellow in Medicine.

Address correspondence to: Lisa S. Westerberg, Karolinska Institutet, Department of Microbiology, Tumor and Cell Biology, Biomedicum, Solnavägen 9, SE-171 65 Stockholm, Sweden. Phone: 46.8.52486833; Email: Lisa.Westerberg@ki.se. Or to: Marton Keszei, Karolinska Institutet, Department of Microbiology, Tumor and Cell Biology, Biomedicum, Solnavägen 9, SE-171 65 Stockholm, Sweden. Phone: 46.8.52486833; Email: Marton.Keszei@ki.se.

1. Skokowa J, Dale DC, Touw IP, Zeidler C, Welte K. Severe congenital neutropenias. *Nat Rev Dis Primers*. 2017;3:17032.
2. Dale DC, Link DC. The many causes of severe congenital neutropenia. *N Engl J Med*. 2009;360(1):3–5.
3. Klein C. Genetic defects in severe congenital neutropenia: emerging insights into life and death of human neutrophil granulocytes. *Annu Rev Immunol*. 2011;29:399–413.
4. Dinauer MC. Primary immune deficiencies with defects in neutrophil function. *Hematology Am Soc Hematol Educ Program*. 2016;2016(1):43–50.
5. van de Vijver E, van den Berg TK, Kuijpers TW. Leukocyte adhesion deficiencies. *Hematol Oncol Clin North Am*. 2013;27(1):101–116, viii.
6. Nemeth T, Mocsai A. Feedback amplification of neutrophil function. *Trends Immunol*. 2016;37(6):412–424.
7. Kolaczkowska E, Kubes P. Neutrophil recruitment and function in health and inflammation. *Nat Rev Immunol*. 2013;13(3):159–175.
8. Lomakina EB, Marsh G, Waugh RE. Cell surface topography is a regulator of molecular interactions during chemokine-induced neutrophil spreading. *Biophys J*. 2014;107(6):1302–1312.
9. Nunoi H, et al. A heterozygous mutation of β-actin associated with neutrophil dysfunction and recurrent infection. *Proc Natl Acad Sci U S A*. 1999;96(15):8693–8698.
10. Record J, et al. Immunodeficiency and severe susceptibility to bacterial infection associated with a loss-of-function homozygous mutation of MKL1. *Blood*. 2015;126(13):1527–1535.
11. Keszei M, Westerberg LS. Congenital defects in neutrophil dynamics. *J Immunol Res*. 2014;2014:303782.
12. Moulding DA, Record J, Malinova D, Thrasher AJ. Actin cytoskeletal defects in immunodeficiency.

Immunol Rev. 2013;256(1):282–299.
13. Procaccio V, et al. A mutation of β-actin that alters depolymerization dynamics is associated with autosomal dominant developmental malformations, deafness, and dystonia. *Am J Hum Genet*. 2006;78(6):947–960.
14. Rivière JB, et al. De novo mutations in the actin genes ACTB and ACTG1 cause Baraitser-Winter syndrome. *Nat Genet*. 2012;44(4):440–444, S1.
15. Beel K, et al. A large kindred with X-linked neutropenia with an I294T mutation of the Wiskott-Aldrich syndrome gene. *Br J Haematol*. 2009;144(1):120–126.
16. Devriendt K, et al. Constitutively activating mutation in WASP causes X-linked severe congenital neutropenia. *Nat Genet*. 2001;27(3):313–317.
17. Ancliff PJ, et al. Two novel activating mutations in the Wiskott-Aldrich syndrome protein result in congenital neutropenia. *Blood*. 2006;108(7):2182–2189.
18. Kim AS, Kakalis LT, Abdul-Manan N, Liu GA, Rosen MK. Autoinhibition and activation mechanisms of the Wiskott-Aldrich syndrome protein. *Nature*. 2000;404(6774):151–158.
19. Rohatgi R, Ho HY, Kirschner MW. Mechanism of N-WASP activation by CDC42 and phosphatidylinositol 4, 5-bisphosphate. *J Cell Biol*. 2000;150(6):1299–1310.
20. Rohatgi R, et al. The interaction between N-WASP and the Arp2/3 complex links Cdc42-dependent signals to actin assembly. *Cell*. 1999;97(2):221–231.
21. Torres E, Rosen MK. Contingent phosphorylation/dephosphorylation provides a mechanism of molecular memory in WASP. *Mol Cell*. 2003;11(5):1215–1227.
22. Cory GO, Garg R, Cramer R, Ridley AJ. Phosphorylation of tyrosine 291 enhances the ability of WASp to stimulate actin polymerization and filopodium formation. Wiskott-Aldrich syndrome protein. *J Biol Chem*. 2002;277(47):45115–45121.
23. Guinamard R, Aspenström P, Fougereau M, Chavrier P, Guillemot JC. Tyrosine phosphorylation of the Wiskott-Aldrich syndrome protein by Lyn and Btk is regulated by CDC42. *FEBS Lett*. 1998;434(3):431–436.
24. Fujimoto H, et al. Flow cytometric method for enumeration and classification of reactive immature granulocyte populations. *Cytometry*. 2000;42(6):371–378.
25. Sørensen O, Arnljots K, Cowland JB, Bainton DF, Borregaard N. The human antibacterial cathelicidin, hCAP-18, is synthesized in myelocytes and metamyelocytes and localized to specific granules in neutrophils. *Blood*. 1997;90(7):2796–2803.
26. Ye Y, et al. The antimicrobial propeptide hCAP-18 plasma levels in neutropenia of various aetiologies: a prospective study. *Sci Rep*. 2015;5:11685.
27. Nauseef WM, Isolation of human neutrophils from venous blood. In: Quinn MT, DeLeo FR, Bokoch GM, eds. *Neutrophil Methods and Protocols*. *Methods in Molecular Biology*; vol 412. Totowa, NJ: Humana Press Inc.; 2007:15–20.
28. Riedl J, et al. Lifeact mice for studying F-actin dynamics. *Nat Methods*. 2010;7(3):168–169.
29. Zhang H, et al. Impaired integrin-dependent function in Wiskott-Aldrich syndrome protein-deficient murine and human neutrophils. *Immunity*. 2006;25(2):285–295.
30. Sakuma C, Sato M, Takenouchi T, Chiba J, Kitani H. Critical roles of the WASP N-terminal domain and Btk in LPS-induced inflammatory response in macrophages. *PLoS One*. 2012;7(1):e30351.
31. Volmering S, Block H, Boras M, Lowell CA, Zarbock A. The neutrophil Btk signalosome regulates integrin activation during sterile inflammation. *Immunity*. 2016;44(1):73–87.
32. Borregaard N, Cowland JB. Granules of the human neutrophilic polymorphonuclear leukocyte. *Blood*. 1997;89(10):3503–3521.
33. Schäffer AA, Klein C. Animal models of human granulocyte diseases. *Hematol Oncol Clin North Am*. 2013;27(1):129–148, ix.
34. Schäffer AA, Klein C. Genetic heterogeneity in severe congenital neutropenia: how many aberrant pathways can kill a neutrophil? *Curr Opin Allergy Clin Immunol*. 2007;7(6):481–494.
35. Belaaouaj A, et al. Mice lacking neutrophil elastase reveal impaired host defense against Gram negative bacterial sepsis. *Nat Med*. 1998;4(5):615–618.
36. von Vietinghoff S, Ley K. Homeostatic regulation of blood neutrophil counts. *J Immunol*. 2008;181(8):5183–5188.
37. The Jackson Laboratory. Mouse Phenome Database. The Jackson Laboratory website. https://phenome.jax.org/strains/jax/664. Accessed July 20, 2018.
38. Wakeman L, et al. Robust, routine haematology reference ranges for healthy adults. *Int J Lab Hematol*. 2007;29(4):279–283.
39. Westerberg LS, et al. Activating WASP mutations associated with X-linked neutropenia result in enhanced actin polymerization, altered cytoskeletal responses, and genomic instability in lymphocytes. *J Exp Med*. 2010;207(6):1145–1152.
40. Park H, Cox D. Cdc42 regulates Fcγ receptor-mediated phagocytosis through the activation and phosphorylation of Wiskott-Aldrich syndrome protein (WASP) and neural-WASP. *Mol Biol Cell*. 2009;20(21):4500–4508.
41. Blundell MP, et al. Phosphorylation of WASp is a key regulator of activity and stability in vivo. *Proc Natl Acad Sci U S A*. 2009;106(37):15738–15743.
42. Boras M, et al. Skap2 is required for β_2 integrin-mediated neutrophil recruitment and functions. *J Exp Med*. 2017;214(3):851–874.
43. DiMilla PA, Stone JA, Quinn JA, Albelda SM, Lauffenburger DA. Maximal migration of human smooth muscle cells on fibronectin and type IV collagen occurs at an intermediate attachment strength. *J Cell Biol*. 1993;122(3):729–737.
44. Snapper SB, et al. Wiskott-Aldrich syndrome protein-deficient mice reveal a role for WASP in T but not B cell activation. *Immunity*. 1998;9(1):81–91.
45. Gupta D, Shah HP, Malu K, Berliner N, Gaines P. Differentiation and characterization of myeloid cells. *Curr Protoc Immunol*. 2014;104:Unit 22F.5.
46. Mócsai A, Zhang H, Jakus Z, Kitaura J, Kawakami T, Lowell CA. G-protein-coupled receptor signaling in Syk-deficient neutrophils and mast cells. *Blood*. 2003;101(10):4155–4163.
47. Schindelin J, et al. Fiji: an open-source platform for biological-image analysis. *Nat Methods*. 2012;9(7):676–682.